Automatic Flaw Detection and Identification for Coiled Tubing
Final Report*

Contracted DOE Laboratory:
Idaho National Laboratory

Principle and Co-Principle Investigators:
Dr. Charles R. Tolle
Dr. Herschel B. Smartt
Mr. Arthur Watkins

Staff Members:
Mr. Timothy McJunkin
Mrs. Karen Miller
Mr. Eric Larson

Industrial Partnership
Tulsa University Coiled Tubing Mechanics Research Consortium
(TUCTMRC)
University of Tulsa
Dr. Steven M. Tipton

August 30, 2006

For further information contact Dr. Charles R. Tolle by email
Charles.Tolle@inl.gov, or Phone (208)526-1895

*This work was supported by the Office of Fossil Energy, U.S. Department of Energy, under the Department of Energy's Idaho Operations Office Contract DE-AC07-05ID14517.

Statement of Problem: Current coiled tubing (CT) field inspection technology is relatively crude, consisting of rolling friction wheels to monitor depth, limited systems which monitor CT diameter and ovality, and magnetic flux leakage systems to identify defects, but with little reliability in identifying the type of defect present (cracks, corrosion) or any dimensional information. CT operates in an extremely severe mechanical environment where large bending strains are combined with significant internal pressure. This can cause diametral growth, wall thinning, ovality, elongation, residual stresses, and low cycle fatigue cracks. Surface defects can shorten operational life spans significantly.

The reliability of CT has been enhanced by extensive refinements to its manufacturing process. CT strings are now making as many as eighty trips into bore holes resulting in a wide variety of service-induced defects. Additionally, there are often long periods of inactivity (storage) during which time corrosion can enhance the damage to the tube surfaces. This extended operational life of the tubing can be partially attributed to laboratory experimentation and theoretical work involving fatigue modeling. Sophisticated plasticity and fatigue damage models predict life for discrete sections along the entire string throughout its service history. However, used CT tends to fail sooner than predicted due to the presence of defects incurred through mechanical damage and/or corrosion. Theoretical/empirical fatigue models could benefit greatly from data concerning the type and dimensions of defects present on the surface of the tubing as defect geometry has a direct impact on the operational life of the tubing, according to results from the Tulsa University Tubing Mechanics Research Consortium (TUCTMRC).

Comparison of New Technology to Existing Technology: New sensing and analysis techniques have a potential for reducing the probability of down-hole CT failures due to low cycle fatigue. Existing CT inspection technology uses Hall probes and electromagnets or permanent magnets to sense defects via magnetic flux leakage (MFL). To further reduce computer-processing power, electronic hardware combines all signals within an inspection quadrant (e.g. one-fourth of the pipe) and the processing/controlling computer records only the maximum strength signal of all the sensors in that quadrant. Combining two quadrants together and recording the maximum values between the two quadrants further reduces the MFL signal storage requirements. Thus, only peak-to-peak signals are stored for offline evaluation. The new equipment and analysis algorithms were prepared as a result of this work to take advantage of recent advances in new computer data acquisition hardware. Computer algorithms were developed to evaluate Hall-effect sensor outputs that could be implemented in real-time to evaluate and determine MFL signals for defect type, size and orientation. The development of sensor and computer algorithms that utilize this type of defect analysis compliments existing TU and TUCTMRC research and development efforts on CT fatigue and lifetime prediction. The interactions between INL and TU have greatly affected both institution's research capabilities within this field of interest, e.g. INL's help during the initial phases of the project greatly increase the reliability and repeatability of TUCTMRC's research apparatus used to collect and study MFL defect signals.

Application and Benefits to Industry: Application of high-speed data acquisition equipment and real-time defect determination and analysis has the propensity when used as input in conjunction with sophisticated plasticity and fatigue damage models to predict the state of the CT string while being used. Such real-time state predictions will reduce down-hole failures, increase CT reliability, and extend CT use. Cost savings due to loss of production and coiled tubing are projected to be $15 to $20M per year.

Summary of Work accomplished: Even though funding was cut based on the original proposal and awarded project, significant work was accomplished during the course of the project. The remainder of this report is made up of 2 parts: one, a letter of support of the project written by our industrial partnership which commends the efforts across the project; and two, three technical papers that were written for publication that resulted from this work. Currently, two of these papers have been published and the third is being submitted for publication as the project closes. Continuation, of this research is being pursued with our industrial partnership, although the realization for further work remains unclear at the writing of this final report.

THE UNIVERSITY of TULSA

DEPARTMENT OF MECHANICAL ENGINEERING

February 9, 2006

Dr. Charles R. Tolle

Idaho National Laboratory
Industrial Technology
P.O. Box 1625, MS2210
Idaho Falls, ID 83415-2210
Phone: 208-526-1895
Email: tollcr@inel.gov

Re: Letter of Support

Dear Dr. Tolle,

We very much appreciate the opportunity to participate as an industry partner in the DOE's Fossil Energy Natural Gas and Oil Technology Partnership. The project entitled: *Automatic Flaw Detection and Identification for Coiled Tubing*, has been of great interest to The University of Tulsa (TU) and its industrial consortium, Tulsa University Coiled Tubing Mechanics Research Consortium (TUCTMRC). This letter serves as formal indication of our desire to our desire to see this project continued for at least the next 3 years.

TU has had an on-going coiled tubing joint industry project for many years. Over that time, TU has developed a sophisticated plasticity and fatigue damage model to predict life for discrete sections along the entire CT string throughout its service history. Currently this model is used for offline evaluation. TU is continuing to empirically refine these models under the guidance and support from the TUCTMRC. These models will be provided and used for the real-time state determination of CT.

The TUCTMRC is comprised of inspection, service, oil, CT manufacturing, and consulting engineering companies. These companies provide project support for TU with industrial "funds-in" contributions and also provide in-kind contributions to this project in the form of samples of coiled tubing etc. They also provide direction within the limitation of the established scope for this project and will provide test-beds to evaluate equipment and algorithms that are developed on this project.

The TUCTMRC held its annual Project Review Meeting at INL during January 2006. This was done because the member companies are very interested in the technology being developed at INL in conjunction with the DOE project. The membership is enthusiastic about what we have learned a great deal during the first stages of this research. We have identified some key concepts with the potential to lead us to field-applicable, real time inspection hardware.

With respect to the proposed study we are willing to commit in-kind funding up to $100,000 per year for this pending budget approvals. This represents our continued efforts on development of a CT defect damage model and steps towards its integration with INL's automated flaw characterization algorithms, for inclusion within a lifetime prediction system for use in the coiled tubing industry world wide. Such an inspection system will have worldwide affects on extending tubing life and reducing costly down hole tube failures which cost the industry $50,000,000 per year.

We believe this study has a strong relevance in the oil and gas industry and we look forward to continuing our participation in the effort with the Idaho National Engineering and Environmental Laboratory.

Sincerely,

Steven M. Tipton

Dr. Steven M. Tipton

The University of Tulsa
TUCTMRC
600 South College Avenue
Tulsa, OK 74104-3189
Telephone: 918-631-2994
Email: smt@utulsa.edu

Published Research Papers:

Characterization of Defects in Coiled Tubing From Magnetic-Flux-Leakage Data

The full-length paper presents observations on use of magnetic-flux-leakage (MFL) data to detect flaws in coiled-tubing (CT) strings. Sixty-six flaws of various shapes and types, ranging from 0.3-mm-deep pits to 9.5-mm-long slots, artificially created in 44.45-mm-outside-diameter pipe, were analyzed. The detection algorithm and the information extracted from the data are described.

Introduction

CT defects reduce CT life and must be detected to prevent costly failures in the field. One method commonly used for CT nondestructive inspection is MFL, where a magnetic field is generated with a coil or permanent magnets and Hall-effect sensors positioned around the CT measure the variation in the field near the CT surface. Flaw characterization is important for failure-prediction models. The size and shape of a flaw influence MFL-signal amplitude and duration and are directly related to expected CT-string life. The full-length paper describes an effective method of detecting flaw signatures in an MFL signal.

Equipment and Processes

A laboratory-scale experimental CT MFL-sensor head was constructed. The coil used to create the field in and around the CT was an 89-mm-long solenoid with a 102-mm inside diameter. One-thousand four-hundred turns of 18-gauge copper wire were wound evenly along the length of the coil. Data presented in the full-length paper were acquired by use of a 5-A direct current in the coil. This current was sufficient to saturate the pipe and permit flaw detection on the inner surface of the CT. Plastic frames, or "shoes," were populated with three ratiometric linear Hall-effect sensors oriented orthogonally in cylindrical coordinates (i.e., radial, longitudinal, and circumferential). Five shoes were distributed circumferentially around approximately one-fourth of the circumference of the CT samples. Artificially created defects were moved past the sensors, with the defect centered approximately on the middle of the five shoes.

Data from the Hall-effect sensors were acquired at a 2000-samples/s rate. A first-order low-pass Butterworth filter with a 100-Hz cutoff frequency was used as a digital filter. The time-series signal was converted into distance vs. amplitude by adjusting for scan velocity and sample rate.

The radial-component signal was used for flaw detection. Signal processing was used for effective flaw detection with few false positives. A matched filter designed for the signature of small defects was correlated with the MFL signal. A matched filter produces a maximum response-to-noise ratio for the desired waveform. For the signal produced by a small flaw, the optimal filter was determined to be the derivative of a Gaussian function with peak-to-peak duration matching that of the minimum flaw to be detected. A threshold value was determined such that it was above the noise-level response but below the response to a small flaw. To reduce false detections further, a minimum width of the response signal also was used. The response width was measured from the first zero crossing on each side of the peak. A minimum width value was chosen to be slightly shorter than the autocorrelation of the matched filter. Values used for the filter and threshold used for the full-length paper were peak-to-peak duration, l_d=3.4 mm, amplitude threshold equal to 2.5, and minimum response width equal to 4.5 mm. The detection algorithm was implemented in software that post-processes data acquired

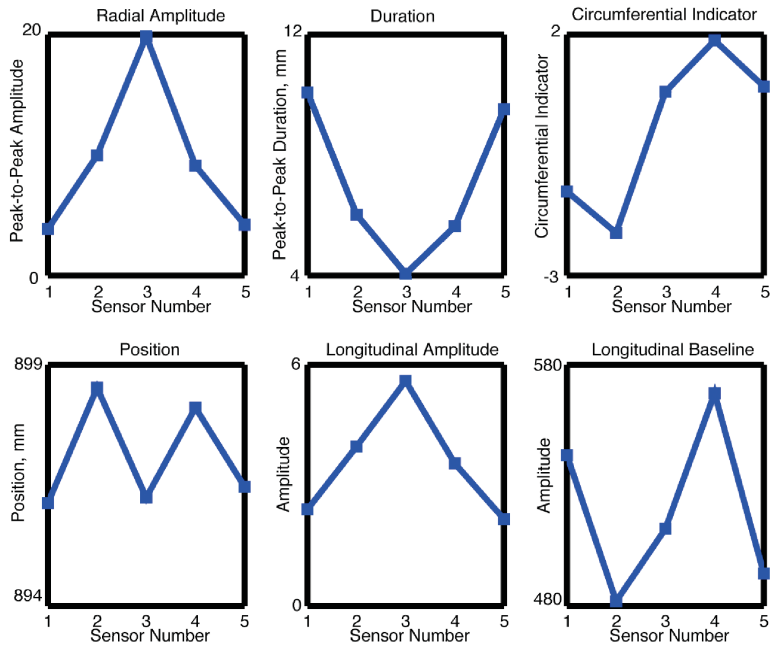

Fig. 1—Information from the five sets of sensors for one defect.

This article, written by Assistant Technology Editor Karen Bybee, contains highlights of paper SPE 100121, "Observations on Characterization of Defects in Coiled Tubing From Magnetic-Flux-Leakage Data," by ***T.R. McJunkin, K.S. Miller,*** *and* ***C.R. Tolle,*** *Idaho Natl. Laboratory, prepared for the 2006 SPE/ICoTA Coiled Tubing and Well Intervention Conference and Exhibition, The Woodlands, Texas, 4–5 April.*

For a limited time, the full-length paper is available free to SPE members at ***www.spe.org/jpt****. The paper has not been peer reviewed.*

with the experimental sensor head. Signal data from the radial component for each sensor position were processed for responses that exceeded the defined thresholds.

At each detection point, additional information was extracted from the signals of all three orthogonal components. The axial (longitudinal) position, p, of the peak is recorded. From the radial-component signal, the local minimum and maximum around the peak of the filter-response location are determined by searching backward and forward in the data as much as four times the peak-to-peak duration, $4l_d$. From the location of the minimum and maximum, the radial-signal amplitude a is recorded as the absolute value of the difference in the amplitude of the local extremes. The absolute value of the difference in axial position of these points is recorded as the signal duration d. From the longitudinal-component signal, the amplitude of the baseline a_b and the peak amplitude minus the baseline a_l are found. The circumferential-component signal has a shape similar to that of the radial component; however, it differs in polarity depending on the sensor position with respect to the detected flaw. A two-point matched filter consisting of one unit impulse in the positive direction and one in the negative direction separated by d is used to analyze the circumferential signal. The peak absolute value of the correlation in the $4l_d$ range around the location of the detected defect determines the magnitude of the circumferential indicator a_c. The sign determines to which side of the sensor the defect is centered. A defect that passes exactly under the sensor would have a value near zero; however, even a small deviation from center produces a signal. The metric for the circumferential sensor is most useful in determining if interpolation between two sensor sets should be used for a flaw that passes between two of the shoes.

Multiple sets of sensors surrounding the pipe may detect the same flaw if the flaw is sufficiently large or wide. The software algorithm attempts to group sensor data if a flaw is detected on multiple shoes. If the position of a flaw on adjacent sensors is within a specified tolerance (8 mm), the data are grouped. Information from all of the sensors is presented in a report and chart. **Fig. 1** shows a chart representation; each parameter is plotted vs. the sensor position. Each sensor number represents one set of sensors at a circumferential position. Sensor Number 3 is centered approximately over the flaw.

Many sizes, shapes, and types of flaws were included in the 66 samples. Flaws were machined, saw cut, impressed, and electrical-discharge machined (EDM). Flaws were created both on the inside and outside of the CT pipes. Sixty-five of 66 flaws were detected automatically by the detection algorithm. One flaw, a 0.58-mm-deep impressed-cone shape, produced a response that was less than the chosen threshold. Choice of a threshold sufficiently low to detect this flaw would have produced a large number of false detections.

Data and Results

Initial observations of radial-signal duration and amplitude from the sensor centered over the flaw indicated several possible correlations for flaw geometry. Radial-signal duration appeared to vary proportionally to the longitudinal length of the flaw. The cross-sectional area of the flaw affected the radial- and longitudinal-signal amplitudes.

First, a set of machined flaws on the outside of two tubes was analyzed in detail. The flaws consisted of ball- and flat-end mill holes of varying depth, flat-end mill slots of varying length and width, and flat-end mill holes of various diameter. Fig. 4 in the full-length paper shows plots of the radial-component amplitude vs. the cross-sectional area and the radial-component duration vs. the longitudinal length of the flaws. A reasonably linear fit is produced on both graphs. The points on the graph of longitudinal length are nearly linear as the length increases. There is more variation in the distribution for shorter-length flaws. The trend is for flaws of various depths to be underestimated and for slots of varying circumferential width to be overestimated by the linear estimation. Note that these flaws have a circumferential dimension greater than the length dimension but have a length dimension sufficiently large that it does not approximate a crack. In a comparison of the cross-sectional area vs. amplitude, there also is a reasonably good fit. However, the apparent variances occur in the flaws with larger areas. The following observations can be made.

- The flaws generated by end mills of varying diameter and slots of varying circumferential width best fit different lines.
- Amplitude increases within the set of flaws of the same cross-sectional area with increasing longitudinal length.

These two observations show that the volume of the flaw affects the amplitude.

A more diverse set of flaws was created in another group of pipe samples by machining, impressing, sawing, and using EDM flaws. A larger variety of shapes was created including ball, cone, and saw cut. EDM flaws were created on both the inside and outside of the pipe. Amplitude vs. cross-sectional area and signal duration vs. flaw length were plotted for these samples. The linear fits from the previous set of flaws were plotted with these data. The fits for the duration of longer (longitudinal) flaws support the linear fit. On average, shorter flaws tend to be oversized by the linear-fit equation of signal duration vs. length. The most-important observations came from the comparison of amplitude to cross-sectional area. The first observation is that internal flaws consistently fall below the trend line. The variation is not extreme, and a conservative estimate of size could assume an internal flaw for sizing purposes. The possibility exists for a separate sensor not sensitive to internal flaws to be used to discriminate between internal and external flaws.

The most serious observation is for the results from saw cuts that approximate cracks. A linear fit for these flaws shows a slope much lower than that of the other flaw types. A crack is a more severe flaw and potential threat to reduce CT life. To be conservative in determining the severity of the detected flaw, the flaw would have to be assumed to be a crack. This would produce the effect that a small pit would be classified as a crack and a CT string would be taken out of service or repaired prematurely. This furthers the argument that the volume of the material missing is related to the amplitude of the response. When the length of the flaw is very small, it is no longer a second-order factor but becomes the primary factor.

Resolving this issue is extremely important for accurately determining the effect of a flaw on CT durability. Unfortunately, signal duration does not discriminate between a pit and a crack (i.e. a small pit does not have a longer signal duration than a crack). As with internal flaws, an independent means for determining a crack from another type of flaw could resolve this issue. There may be some potential for discrimination by use of the amplitude distribution with respect to the circumferentially distributed sensors.

Conclusions

From the data from 65 artificial flaws, observations include that for flaws with length on the order of 2.5 mm and larger, the peak-to-peak amplitude of the radial component of the MFL is roughly proportional to the cross-sectional area. The longitudinal length of the flaw is proportional to the peak-to-peak duration of the radial component of the MFL for flaws greater than 3 mm. There are remaining issues with respect to sizing flaws with low total volume. An analysis of the variation of amplitude with respect to the circumferential position of the sensor to the flaw shows some possibility that better circumferential resolution could aid in differentiating cracks from pits. JPT

SPE-100121-PP

Observations on Characterization of Defects in Coiled Tubing From Magnetic-Flux-Leakage Data

Timothy R. McJunkin, Idaho National Laboratory; Karen S. Miller, Idaho National Laboratory; and Charles R. Tolle, Idaho National Laboratory

Copyright 2006, Society of Petroleum Engineers

This paper was prepared for presentation at the 2006 SPE/ICoTA Coiled Tubing and Well Intervention Conference and Exhibition held in The Woodlands, TX, U.S.A., 4–5 April 2006.

This paper was selected for presentation by an SPE Program Committee following review of information contained in a proposal submitted by the author(s). Contents of the paper, as presented, have not been reviewed by the Society of Petroleum Engineers and are subject to correction by the author(s). The material, as presented, does not necessarily reflect any position of the Society of Petroleum Engineers, its officers, or members. Papers presented at SPE meetings are subject to publication review by Editorial Committees of the Society of Petroleum Engineers. Electronic reproduction, distribution, or storage of any part of this paper for commercial purposes without the written consent of the Society of Petroleum Engineers is prohibited. Permission to reproduce in print is restricted to an abstract of not more than 300 words; illustrations may not be copied. The abstract must contain conspicuous acknowledgment of where and by whom the paper was presented. Write Librarian, SPE, P.O. Box 833836, Richardson, TX 75083-3836, U.S.A., fax 01-972-952-9435.

Abstract

This paper presents observations on the sizing of automatically detected artificial flaws in coiled tubing samples using magnetic-flux-leakage data. Sixty-six artificial flaws of various shapes and types, ranging from 0.30 mm deep pits to slots with length of 9.5 mm, in 44.45 mm outer diameter pipe were analyzed. The detection algorithm and the information automatically extracted from the data are described. Observations on the capabilities and limitations for determining the size and shape of the flaws are discussed.

Introduction

Defects in coiled tubing (CT) degrade the longevity of the CT and, therefore, need to be detected to prevent costly failures in the field. One commonly used method for nondestructively examining CT is magnetic flux leakage (MFL), where a magnetic field is generated with a coil or permanent magnets and Hall-effect sensors located around the CT measure the variation in the field near the surface of the CT. The size, shape, and location of the flaws are an important attribute in determining the point of failure. Characterizing flaws is important to closing the loop on failure prediction models[1]. The size and shape of flaw determines the severity index, developed at the University of Tulsa and is directly related to the expected life of a CT string.

This paper presents the algorithm for automatically extracting information from the MFL signals. An effective method for detecting the signature of flaws in the MFL signal has been

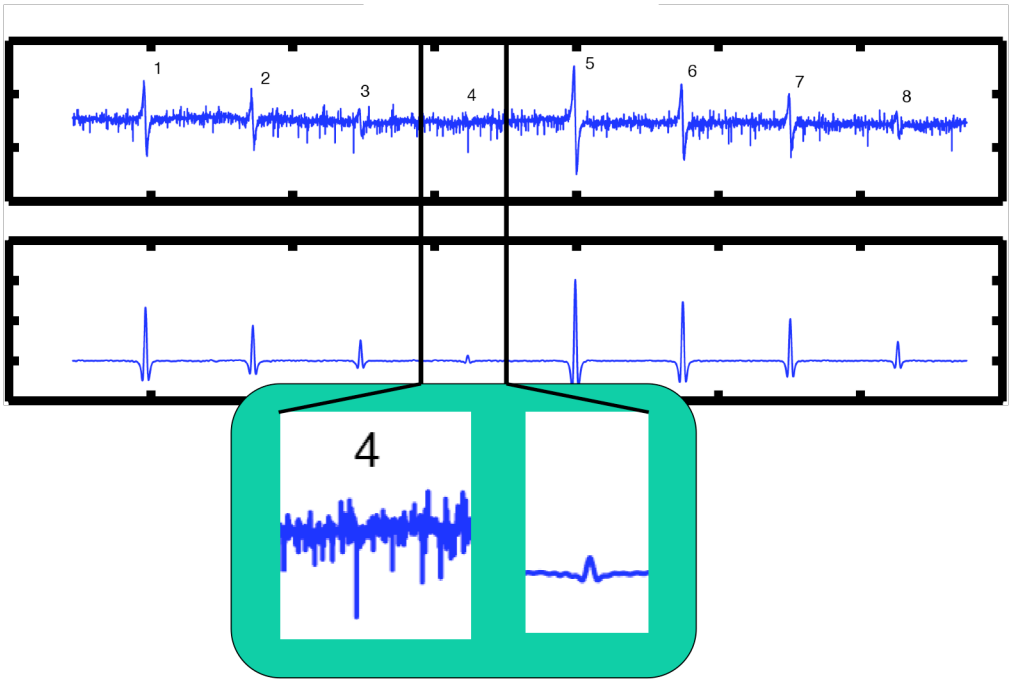

Figure 1. Example of the capabilities of the designed matched filter at maximizing the signal to noise ratio from the radial component of the MFL sensor. In this example the Butterworth pre-filter stage has been omitted. The top signal shows an unfiltered radial component signal of a CT sample with artificial flaws of various sizes. The middle row shows the response of the matched filter to the signal. The bottom signals show an enlargement of the signal (left) and filter response (right) to the smallest flaw.

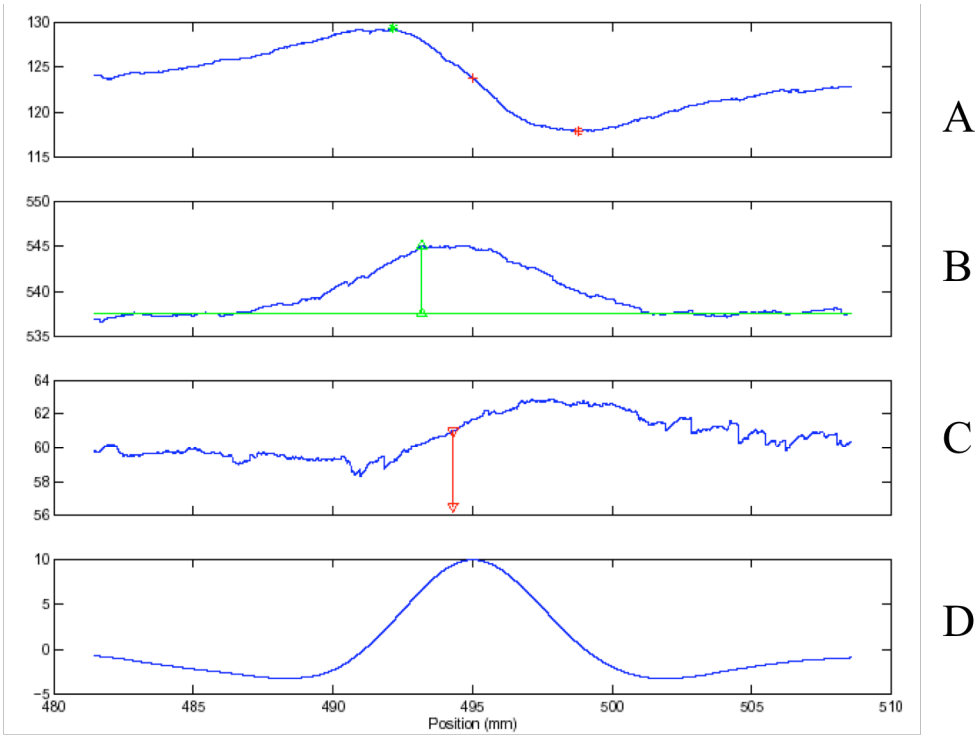

Figure 2. The three orthogonal components of the MFL field at a defect and the parameters that are collected for each component are shown. A) The radial component with the position of the center of the signal and the maximum and minimum point on the signal. B) The axial or longitudinal component shown with the base line (horizontal line) and amplitude above the baseline. C) The circumferential signal with an arrow indicating the amplitude and direction of the indication. D) The output of the matched filter applied to the radial component.

developed[2] and is summarized. In support of failure prediction models, this paper presents the currently observed capabilities of determining the type, size, and severity of flaws present in coiled tubing from MFL. The size and shape of the flaw influences the amplitude and duration of the MFL signals. The extent to which the flaws can and cannot be characterized is discussed. Presentations of the primary issue in discriminating crack type flaws from other less serious flaws conclude with the possible paths forward for resolving the issue.

Description and Application of Equipment and Processes

To collect MFL data, a laboratory scale experimental CT MFL sensor head has been constructed. The coil used to create the field in and around the CT is an 89 mm long solenoid with a 102 mm inner diameter. There are 1400 revolutions (turns) of 18 gauge copper wire wound evenly along the length of the coil. Data presented in this paper was acquired using 5 A direct current in the coil. This level is adequate to saturate the pipe and allow detection of flaws on the inner surface of the CT. Plastic frames, "shoes", were populated with 3 ratiometric linear Hall-effect sensors oriented in each of the orthogonal components for cylindrical coordinates: radial, longitudinal (axial), and circumferential. Five shoes where distributed circumferentially around approximately one fourth the circumference of the CT samples. Artificial defects were run by the sensors, with the defect nominally centered on the middle of the 5 shoes. For experimental convenience, the magnet and sensors are moved with a linear slide driven by a stepper motor.

Data from the Hall effect sensors was acquired with a digital acquisition card sampling each single at a rate of 2000 samples/s. A first-order low pass Butterworth filter with a cutoff frequency of 100Hz was applied as a digital filter in software in all but one example in this paper. The time series signal was converted to a distance versus amplitude by adjusting for scan velocity and sample rate.

The radial component signal was utilized for flaw detection. Signal processing was applied to allow for effective detection of flaws with few false positives. A matched filter designed for the signature of small defects was correlated with the MFL signal. A matched filter produces a maximum ratio of response to the desired waveform to that of noise. For the signal produced by a small flaw, the optimal filter was determined to be the derivative of a Gaussian function with the peak-to-peak duration matching that of a minimum flaw that is to be detected[2]. Although the filter is not optimized for larger flaws the shape of their signal is close enough and amplitude sufficient to allow detection. The response produces a positive pulse in the output of the filter when a flaw signal overlaps the signal. A threshold value was heuristically determined such that it was above the noise level response but below the response to a small flaw. To further reduce false detections a minimum width of the response signal was also implemented. The width of the response was measured from the first zero crossing on each side of the peak. A minimum width value was chosen to be slightly shorter than the autocorrelation of the matched filter. The values used for the filter and threshold used for this paper are:

- l_d – peak-to-peak duration of $h(n)$ -- 3.4 mm

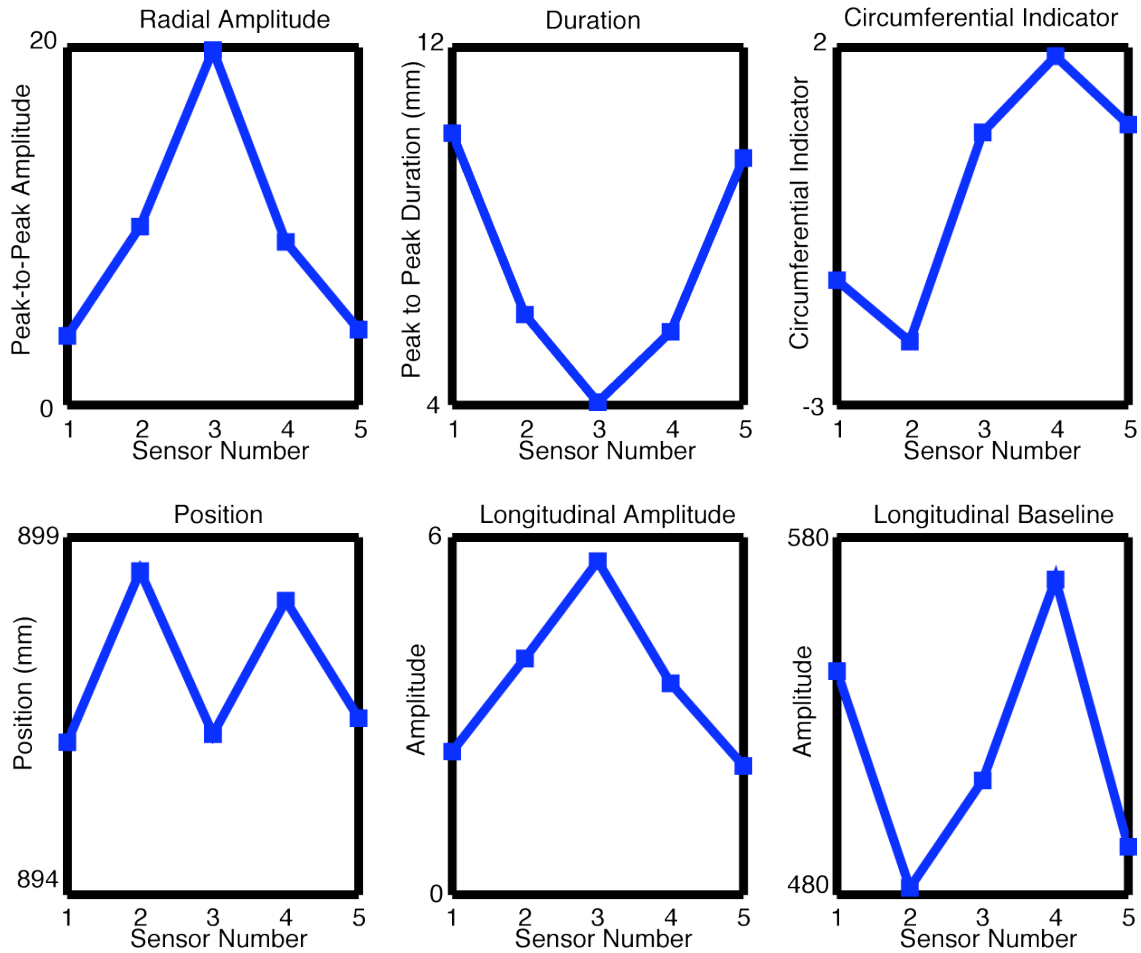

Figure 3. Combined information from the five sets of sensors for one defect. Each sensor number represents one set of sensors at a circumferential position. The flaw was nominally aligned on sensor number 3.

- T_A – amplitude threshold – 2.5
- T_W – minimum response width – 4.5 mm

The function implementing the filter is

$$h(n) = -2\kappa n e^{-(\kappa n)^2}$$

$$\kappa = \frac{\upsilon T\sqrt{2}}{l_d}$$

n is the sample number

T is the sample period (s)

υ is the translation velocity (mm/s)

l_d is the peak-to-peak duration (mm).

The output response at a location in the sampled signal is

$$\nu(n) = \sum_{i=-L}^{L} s(i+n)h(i)$$

with L set to a reasonable length for the filter. We chose a number of samples equivalent to two times l_d, or L is equivalent to the nearest integer to l_d divided by the product of the velocity and sample period.

The detection algorithm was implemented in software that post-processes data acquired with the experimental sensor head. Signal data from the radial component for each sensor position was processed for responses that exceed the defined thresholds. Figure 1 shows the capability of the matched filter in discriminating a flaw from the noise even when the signal from the flaw is buried in the noise (flaw 4). This example uses data where the Butterworth filter was not performed on the data before applying the matched filter, to emphasize the matched filter's capability to reject noise.

At each point that detection occurs, additional information is extracted from the signals of all three orthogonal components. The information abstracted from the signals is shown in Figure 2. The axial (longitudinal) position, p, of the peak of the response is recorded. From the radial component signal the local minimum and maximum around the peak of the filter response location is determined by searching backward and forward in the data as much as $4l_d$. From the minimum and maximum location, the radial signal amplitude, a_r, is recorded as the absolute value of the difference in the amplitude of the to local extremes. The absolute value of the

difference in axial position of these points is recorded as the duration, d, of the signal. From the longitudinal component signal, the amplitude of the baseline, a_b, and the peak amplitude minus the baseline, a_l, are found. The circumferential component signal has a shape similar to that of the radial component; however, it differs in polarity depending on the sensor's position with respect to the detected flaw. A two point matched filter consisting of one unit impulse in the positive direction and one in the negative direction separated by d is used to analyze the circumferential signal. The peak absolute value of the correlation in the $4l_d$ range around the location of the detected defect determines the magnitude of the circumferential indicator, a_c. The sign determines to which side of the sensor the defect is centered. A defect that passes precisely under the sensor would have a value of near zero; however, only a small deviation from center produces a signal. The metric for the circumferential sensor is most useful in determining whether some interpolation between two sensor sets for a flaw that passes between two of the shoes around the pipe should be used.

Multiple sets of sensors surrounding the pipe may detect the same flaw if the flaw is large enough or wide enough. The software algorithm attempts to group sensor data if a flaw is detected on multiple shoes. If the position of a flaw on adjacent sensors is within a specified tolerance of one another, they are grouped. For the data processed for this paper, we used a tolerance of 8 mm to account for possible offsets between the sensors shoes. The combined information from all of the sensors for a flaw is presented in a report and chart. Figure 3 represents the chart representation of the information, each parameter plotted versus the sensor position (sensor number three nominally centered over the flaw).

With the ability to detect and abstract information from the data taken with the sensors, we proceed to describing the observations made on 66 artificial flaws inserted into samples of sections of coiled tubing. The flaws included many sizes, shapes, and types of flaws. Flaws were machined, saw cut, impressed, and electrical discharge machined (EDM). Flaws were included both on the outside and inside of the CT pipes. 65 of 66 flaws were automatically detected with the detection algorithm. The one remaining flaw, 0.58 mm deep impressed cone shape, produced a response to the matched filter but was below the chosen threshold. Choosing a threshold low enough to detect this flaw would have produced a large increase in false detections.

Presentation of Data and Results

From initial observations of the radial signal duration and the radial signal amplitude using only the sensor centered over the flaw, there were several possible correlations to the flaw geometry. The duration of the radial signal appeared to vary proportionally to the longitudinal length of the flaw. The cross-sectional area of the flaw was associated with the amplitude of the radial and longitudinal signals.

A set of machined flaws inserted into the outside of two tubes was analyzed in detail first. The flaws consisted of ball and flat end mill holes of varying depth; flat end mill slots of varying length and widths; and flat end mill holes of various diameters. Details and summary of abstracted data of all of the flaws are contained in Appendix A. Figure 4 shows the graph of the radial component amplitude versus the cross-sectional area and the radial component duration versus the longitudinal length of the flaws. A reasonable linear fit is produced on both graphs (R^2 values of 0.955 on the amplitude graph and 0.925 on the duration graph). The points on the length graph are nearly exactly linear as the length increases. There is more variation in the distribution for flaws of shorter length. The trend is for flaws of various depths to be underestimated by applying the linear estimation and for slots of varying circumferential width to be over estimated. Note these flaws have a circumferential dimension of greater than the length dimension but have a length dimension large enough that it does not approximate a crack. In a comparison of the cross-sectional area versus amplitude there is also a reasonably good fit. However, the apparent variances occur in the larger area flaws. Two observations are made: 1. The flaws that are generated by end mills of varying diameter and slots of varying circumferential width would best fit different lines. 2. There is an increase in amplitude within the set of flaws of the same cross-sectional area due to increasing longitudinal

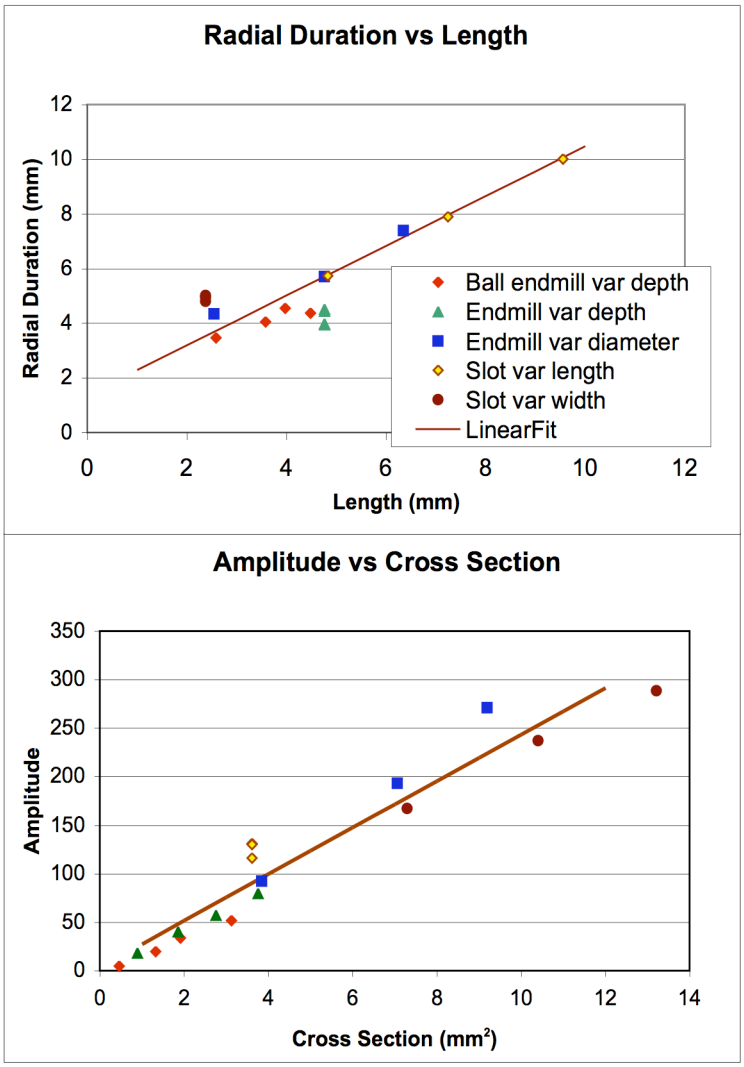

Figure 4. Comparison of duration of the radial signal to the length of flaws and the amplitude to the cross-sectional area. Least squares linear fit for each is shown. Flaws are all external machined flaws.

length. These two observations show that the volume of the flaw has some effect on the amplitude (i.e. there is a second order effect on the amplitude due to the volume of material absent in flaws created with mill tool diameters between 2.38mm and 6.35 mm. These results present a fairly straightforward picture.

The next set of samples complicates the picture. A more diverse set of flaws were inserted in additional pipes by machining, impressing, sawing and EDM. A larger variety of shapes were used including: ball, cone and saw cut. EDM flaws were inserted on both the inside and outside of the pipe. The plots of the comparison of amplitude to cross-sectional area and signal duration to length of flaws were completed on these samples as well. Figure 5 contains the graphs of the results for these flaws. The linear fits from the previous set of flaws were plotted with this data. The fits for the duration of longer (longitudinal) flaws support the linear fit. Shorter flaws tend, on average, to be oversized by applying the linear fit equation of related signal duration to length. The most important observations were made from the comparison of amplitude to cross-sectional area. The first is that internal flaws fall consistently below the trend line. The variation is not extreme and a conservative estimate of size could assume an internal flaw for sizing purposes. A possibility exists for a separate sensor that would not be sensitive to internal flaws be used to discriminate between internal and external flaws.

The more serious observation is for the results from saw cuts that approximate cracks. A linear fit for these flaws shows a slope much lower than that of the other types of flaws. A crack is arguably a more severe type of flaw for reducing the longevity of a CT string. To be conservative in attempting to determine the severity of a detected flaw, it would have to be assumed to be a crack. This would produce the effect that a small pit would be classified as a crack and a CT string be taken out of service or repaired prematurely. This result furthers the argument that the volume of the material missing is related to the amplitude of the response. When the length of the flaw is very small, it is no longer a second order factor but becomes the primary factor.

Resolving this issue is extremely important for accurately determining the severity of a flaw's effect on the CT durability. Unfortunately, the duration of the signal does not discriminate between a pit and a crack (i.e. a small pit does not have a longer duration than a crack). As with the internal flaws an independent means for determining a crack versus another type of flaw could potentially resolve this issue. A subtle observation of the amplitude versus the circumferential position of the sensors distributed around the pipe is shown in

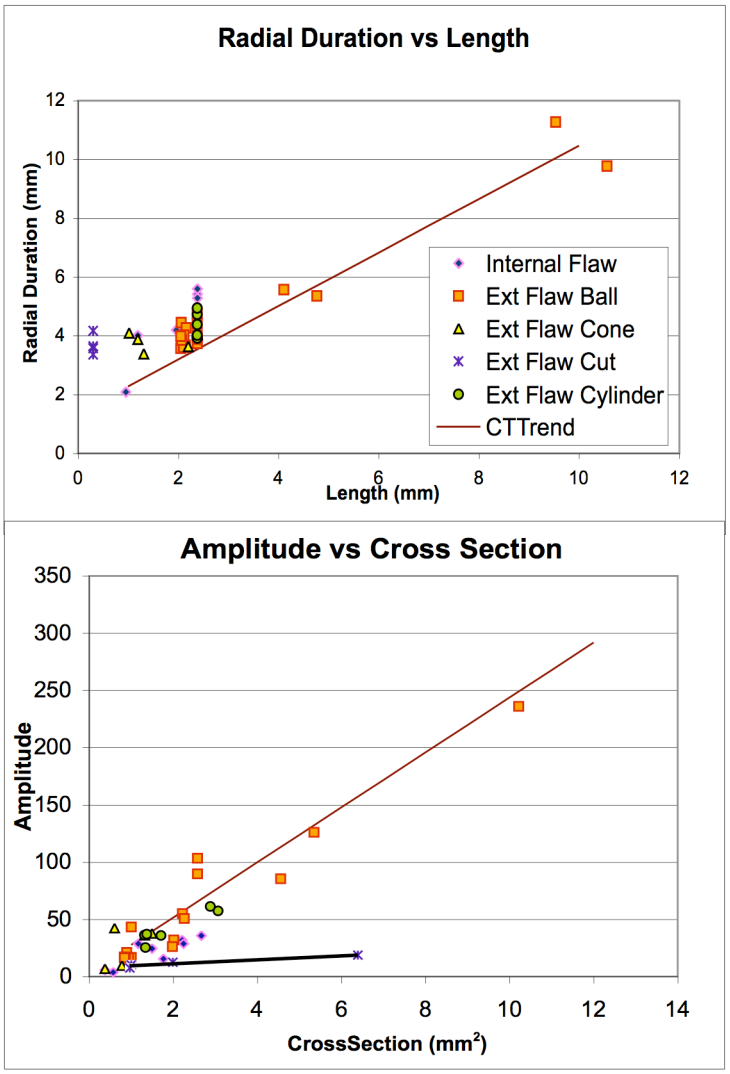

Figure 5. Comparison of duration and amplitude to a more diverse set of flaw including internal, external, and saw cuts.

Figure 6. The decrease in amplitude of the MFL signal out circumferentially from the center of the flaw is less on the saw cut as compared to the ball end-mill produced pit that produces approximately the same amplitude response on the center sensor. There may be some potential to discriminate using the distribution of the amplitude with respect to the circumferentially distributed sensors. This is the most promising observation in the current data sets for a potential to resolve this issue.

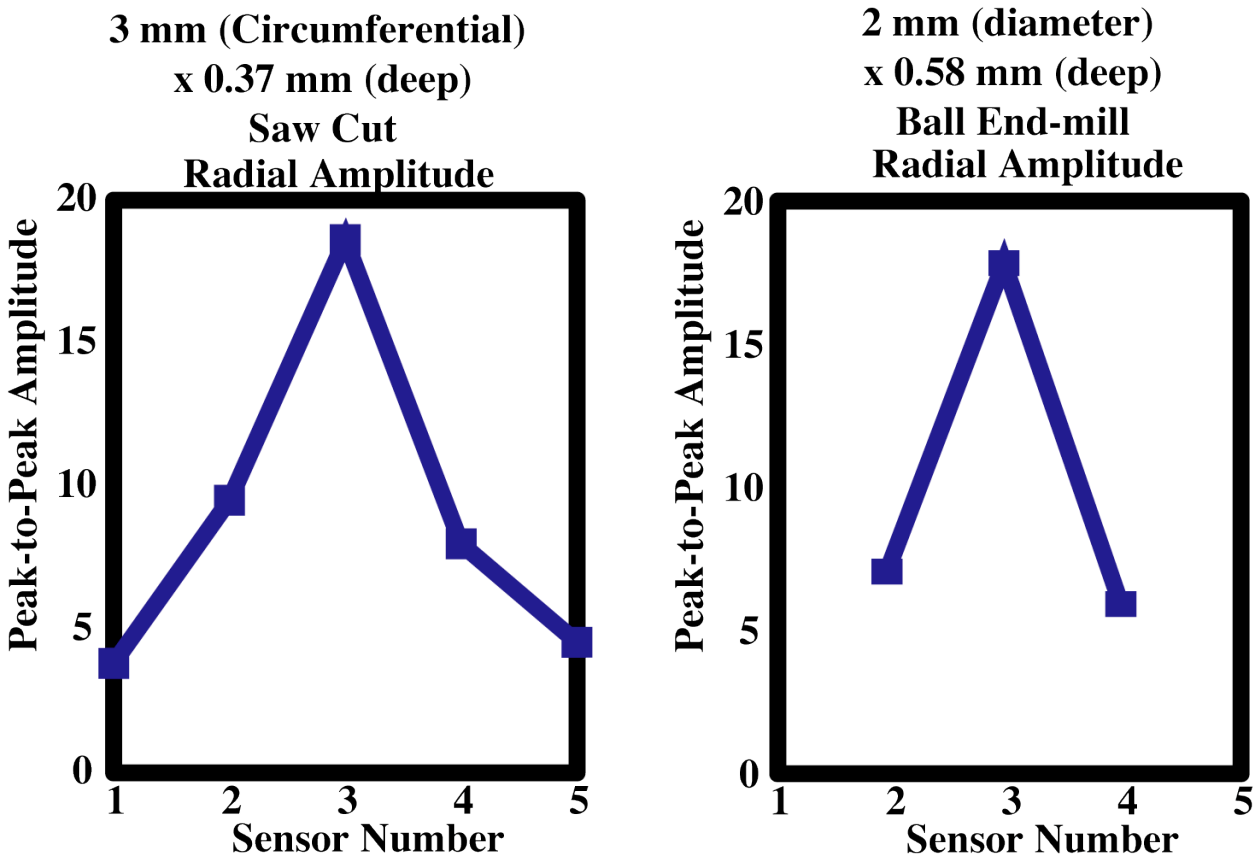

Figure 6. Comparison of the amplitude of a simulated pit and simulated crack. The amplitude of the radial component is shown versus the circumferential position of the sensor shoes. Although each has approximately the same amplitude on the center sensor the amplitude of the pit decreases faster and is not even detected at sensor numbers 1 and 5.

Conclusions

This paper presented the observations on the ability to determine geometry of flaws in coiled tubing from MFL data. An algorithm to effectively automatically detect and extract information from the flaw data with a matched filter was described. From the resulting data points for 65 artificial flaws, observations were made about the signals versus flaw length and cross-sectional area. For flaws with length on the order of the 2.5 mm and larger the peak-to-peak amplitude of the radial component of the MFL is roughly proportional to the cross-sectional area. The longitudinal length of the flaw is proportional to the peak-to-peak duration of the radial component of the MFL for flaws greater than 3 mm. There are remaining issues with respect to sizing flaws with low total absent volume. An analysis of the variation of amplitude with respect to the circumferential position of the sensor to the flaw shows some possibility that better circumferential resolution could pay a dividend in resolving cracks from pits. It is likely that a more robust approach may be to apply a sensor that is sensitive to cracks but not to pits. One such possibility is the "Föster" method[3]. Future research will include implementing this method.

Acknowledgements

We gratefully acknowledge the partnership of the University of Tulsa and the University of Tulsa Coiled Tubing Mechanics Research Consortium in the project. We specially thank Rod Stanley for the suggestion of the Föster method. This work was supported by the Office of Fossil Energy, U.S. Department of Energy, under the Department of Energy's Idaho Operations Office Contract DE-AC07-05ID14517.

References

1-Tipton, S.M.:"Multiaxial Plasticity and Fatigue Life Prediction in Coiled Tubing," in Fatigue Lifetime Predictive Techniques: 3rd Volume, ASTM STP 1292, American Society for Testing and Materials, 1996, pp. 283-304.

2-McJunkin, T.R, et al.: "Detection of Coiled Tubing Defects Using Matched Filter Algorithm", NDE&T International, Submitted September 2005.

3-Föster F.: "On the Way from "know-how" to the "know-why" in Magnetic Leakage Field Method of Nondestructive Testing," Chinese Journal of NDT, 1997, 19 (11), pp. 347-350.

Appendix A

This appendix provides the measurements of the signals from each of the flaws analyzed in the article. Each row contains a description of the artificial defect and a summary of information extracted from the MFL signals. The graphs include the data from each of the five sensor sets arranged around approximately one fourth the circumference of the CT samples. The data included here is from left to right: amplitude of the radial component measured from highest to lowest point on the flaw signal, the duration of the signal from highest to lowest point measured in millimeters, the value of the circumferential component indicator, and the amplitude of the longitudinal (axial) component measured from the baseline amplitude of the signal.

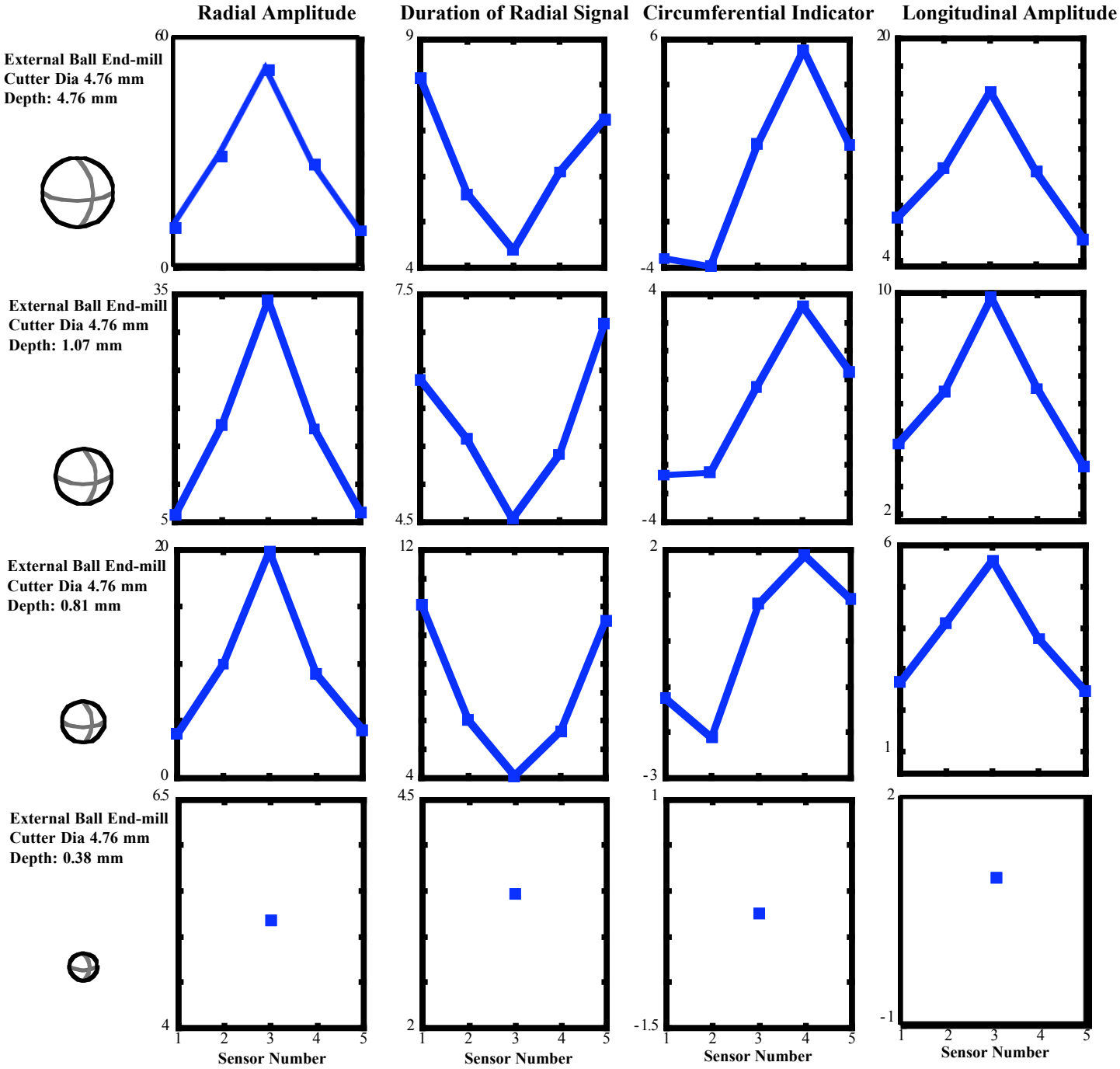

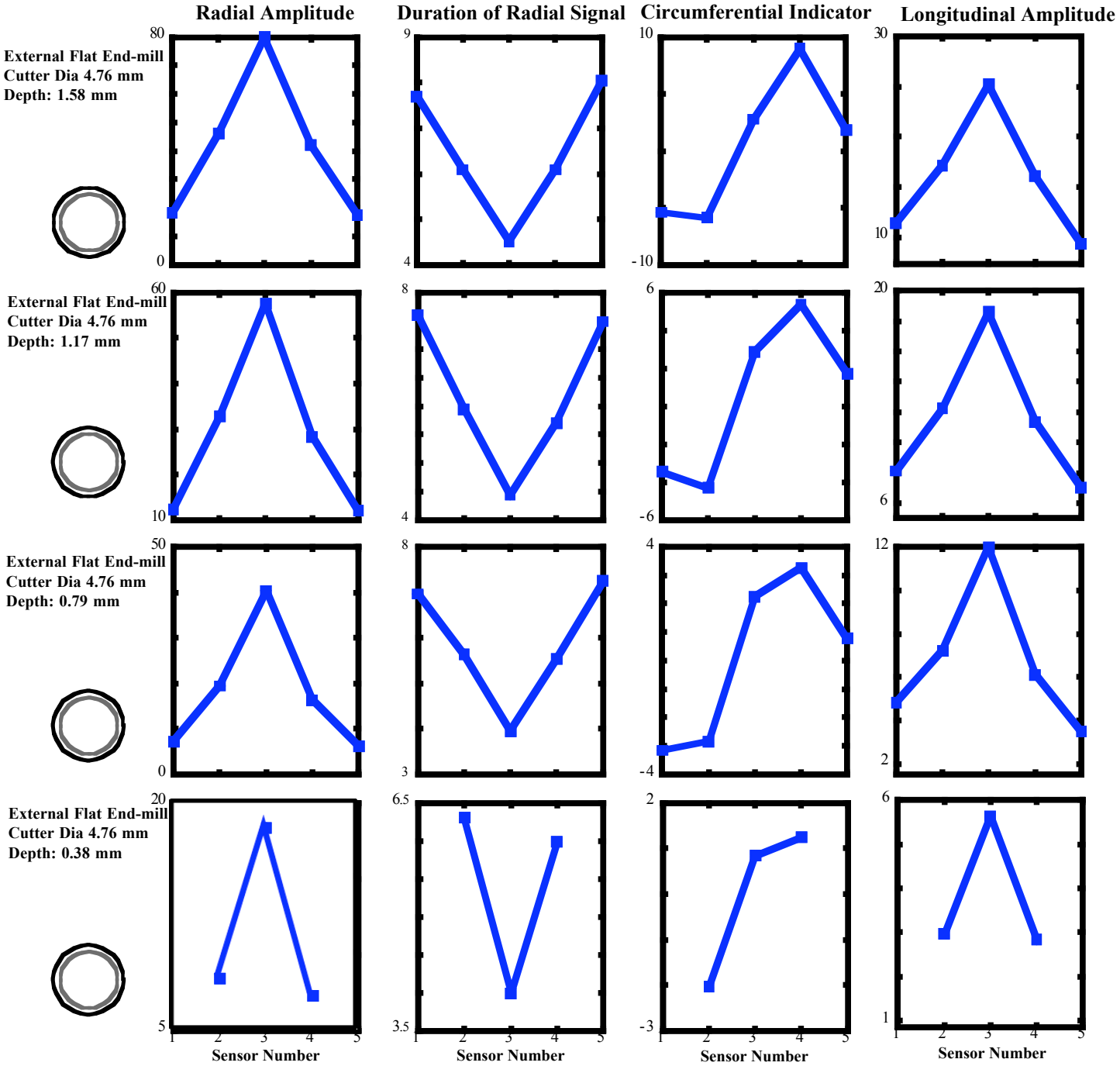
Radial Amplitude
Duration of Radial Signal
Circumferential Indicator
Longitudinal Amplitude
External Flat End-mill
Cutter Dia 4.76 mm
Depth: 1.58 mm
External Flat End-mill
Cutter Dia 4.76 mm
Depth: 1.17 mm
External Flat End-mill
Cutter Dia 4.76 mm
Depth: 0.79 mm
External Flat End-mill
Cutter Dia 4.76 mm
Depth: 0.38 mm
80
0
9
4
10
-10
30
10
60
10
8
4
6
-6
20
6
50
0
8
3
4
-4
12
2
20
5
6.5
3.5
2
-3
6
1
1 2 3 4 5
Sensor Number

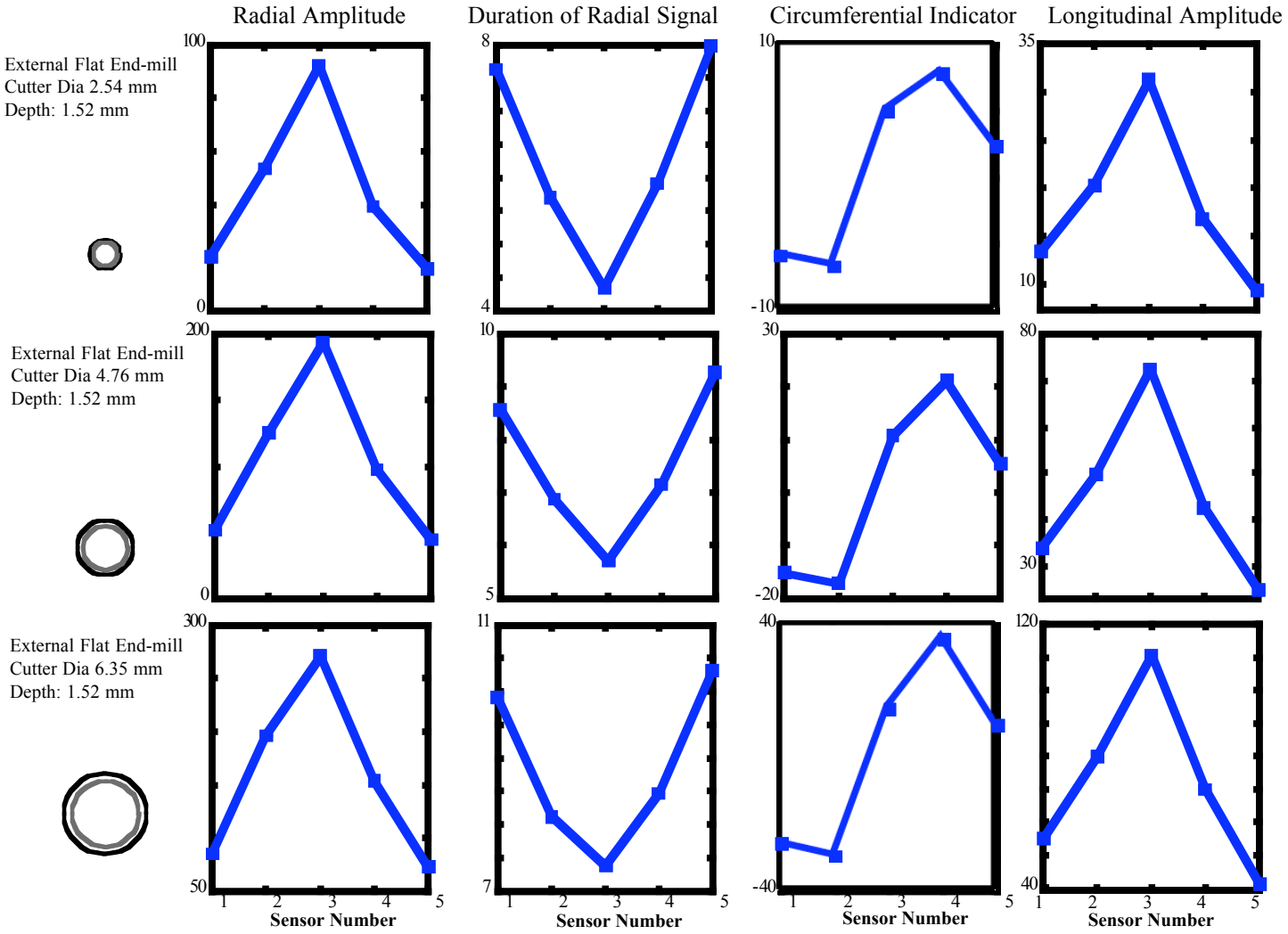
Radial Amplitude
Duration of Radial Signal
Circumferential Indicator
Longitudinal Amplitude
External Flat End-mill
Cutter Dia 2.54 mm
Depth: 1.52 mm
External Flat End-mill
Cutter Dia 4.76 mm
Depth: 1.52 mm
External Flat End-mill
Cutter Dia 6.35 mm
Depth: 1.52 mm
100
0
8
4
10
-10
35
10
200
0
10
5
30
-20
80
30
300
50
11
7
40
-40
120
40
1 2 3 4 5
Sensor Number

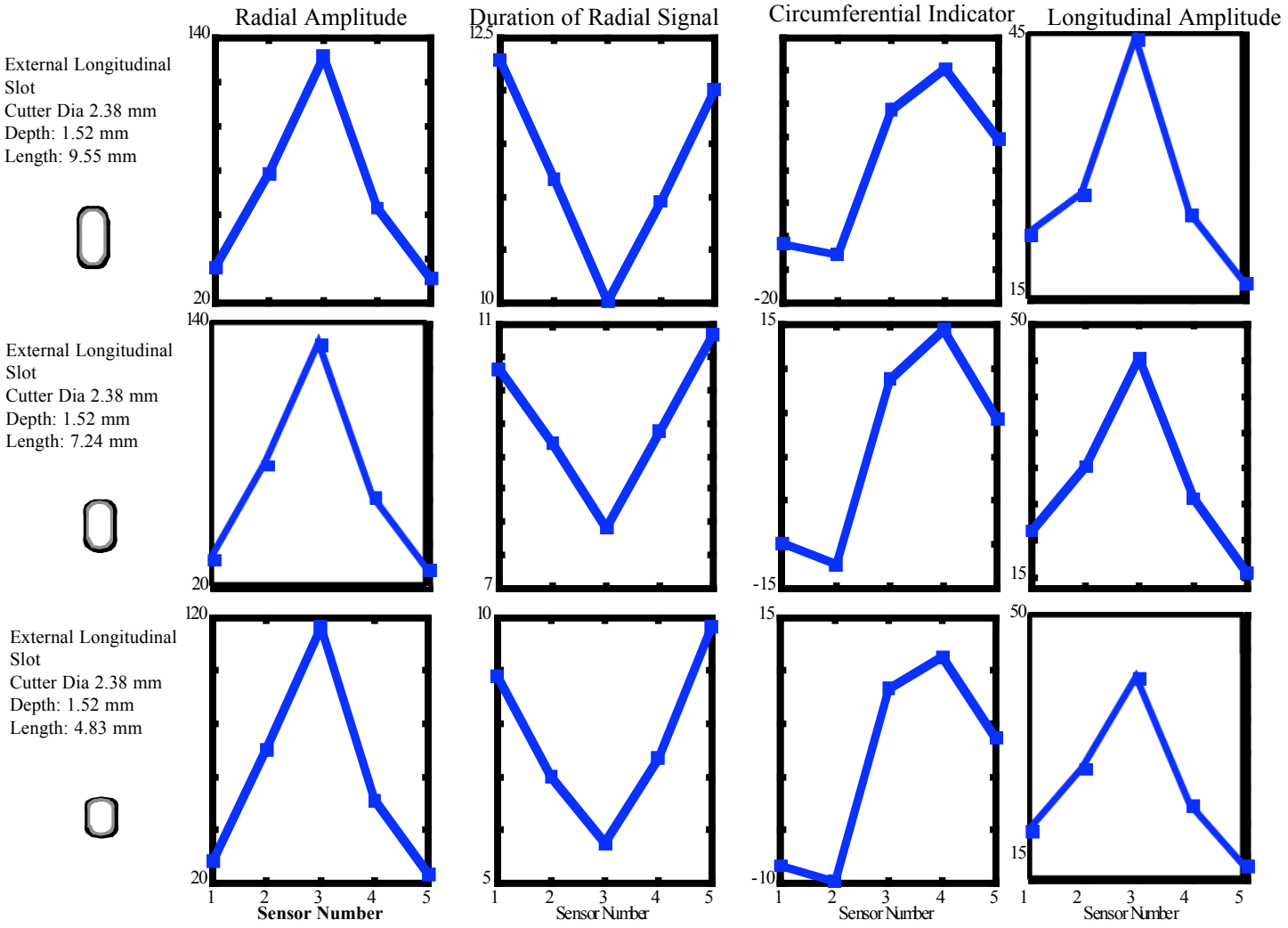
Radial Amplitude
Duration of Radial Signal
Circumferential Indicator
Longitudinal Amplitude
External Longitudinal Slot
Cutter Dia 2.38 mm
Depth: 1.52 mm
Length: 9.55 mm
External Longitudinal Slot
Cutter Dia 2.38 mm
Depth: 1.52 mm
Length: 7.24 mm
External Longitudinal Slot
Cutter Dia 2.38 mm
Depth: 1.52 mm
Length: 4.83 mm
140
20
12.5
10
45
15
-20
140
20
11
7
15
-15
50
15
120
20
10
5
15
-10
50
15
1 2 3 4 5
Sensor Number

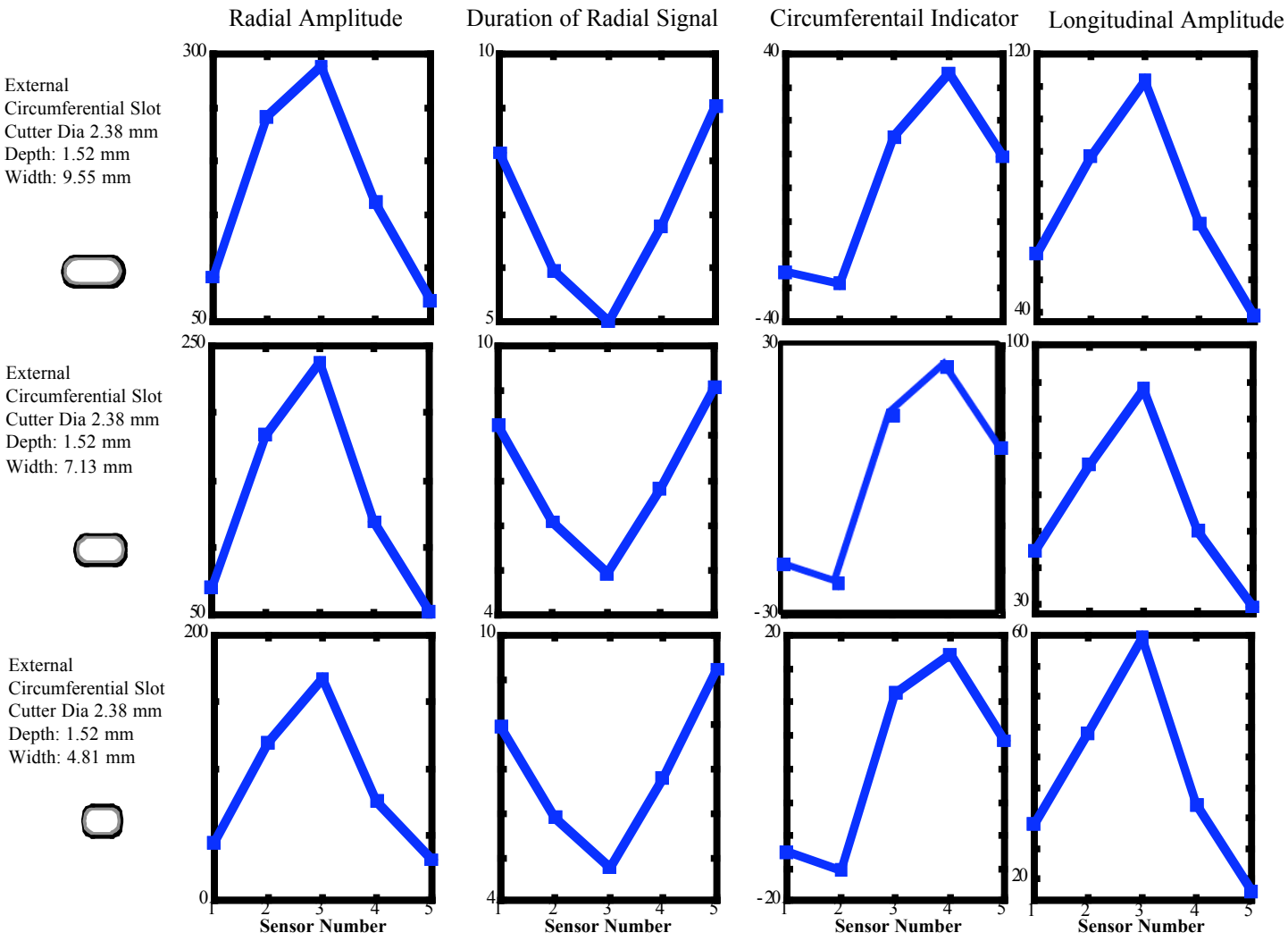
Radial Amplitude
Duration of Radial Signal
Circumferentail Indicator
Longitudinal Amplitude
External
Circumferential Slot
Cutter Dia 2.38 mm
Depth: 1.52 mm
Width: 9.55 mm
External
Circumferential Slot
Cutter Dia 2.38 mm
Depth: 1.52 mm
Width: 7.13 mm
External
Circumferential Slot
Cutter Dia 2.38 mm
Depth: 1.52 mm
Width: 4.81 mm
300
50
10
5
40
-40
120
40
250
50
10
4
30
-30
100
30
200
0
10
4
20
-20
60
20
1 2 3 4 5
Sensor Number

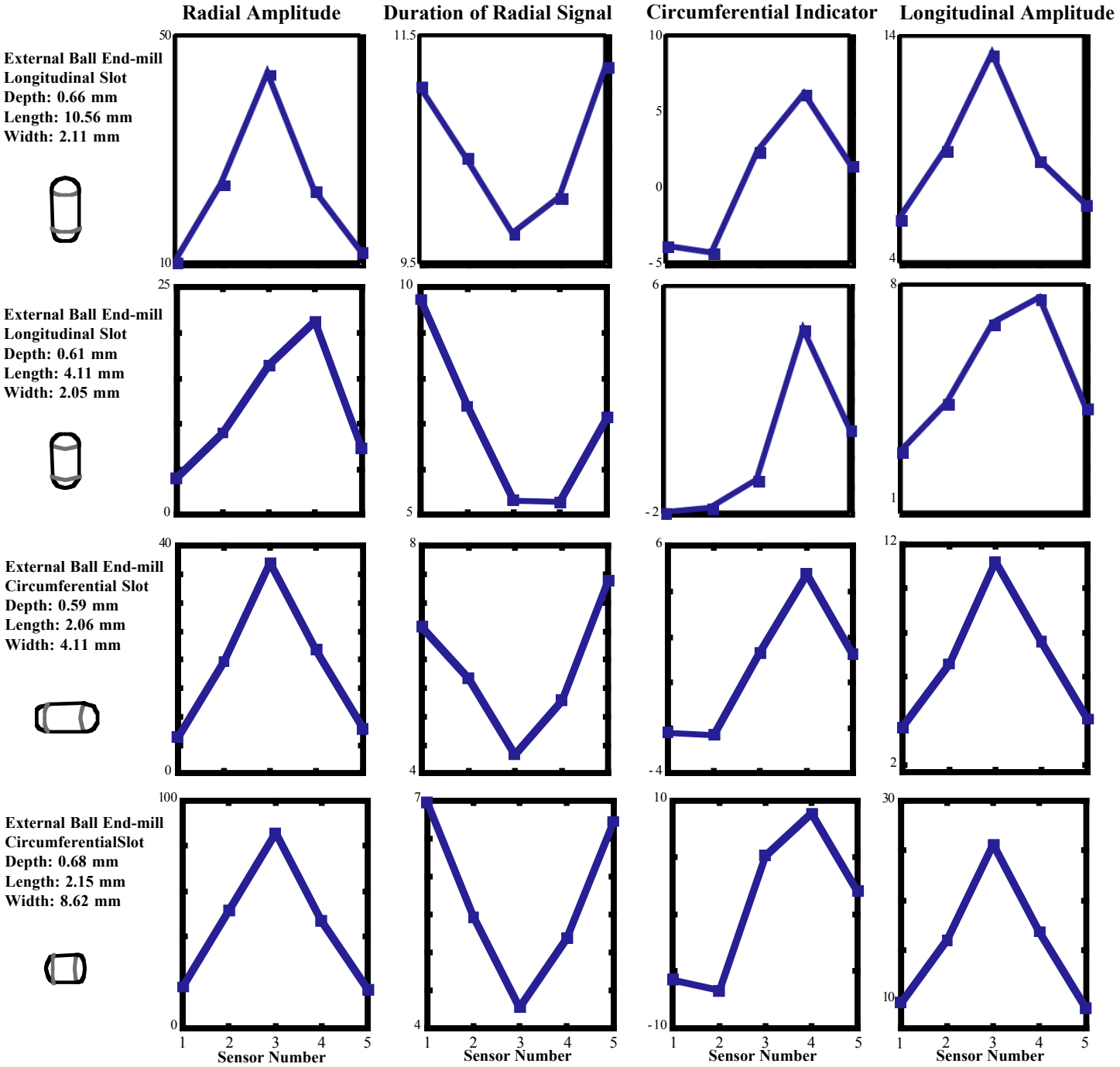
Radial Amplitude
Duration of Radial Signal
Circumferential Indicator
Longitudinal Amplitude
External Ball End-mill
Longitudinal Slot
Depth: 0.66 mm
Length: 10.56 mm
Width: 2.11 mm
External Ball End-mill
Longitudinal Slot
Depth: 0.61 mm
Length: 4.11 mm
Width: 2.05 mm
External Ball End-mill
Circumferential Slot
Depth: 0.59 mm
Length: 2.06 mm
Width: 4.11 mm
External Ball End-mill
CircumferentialSlot
Depth: 0.68 mm
Length: 2.15 mm
Width: 8.62 mm
Sensor Number

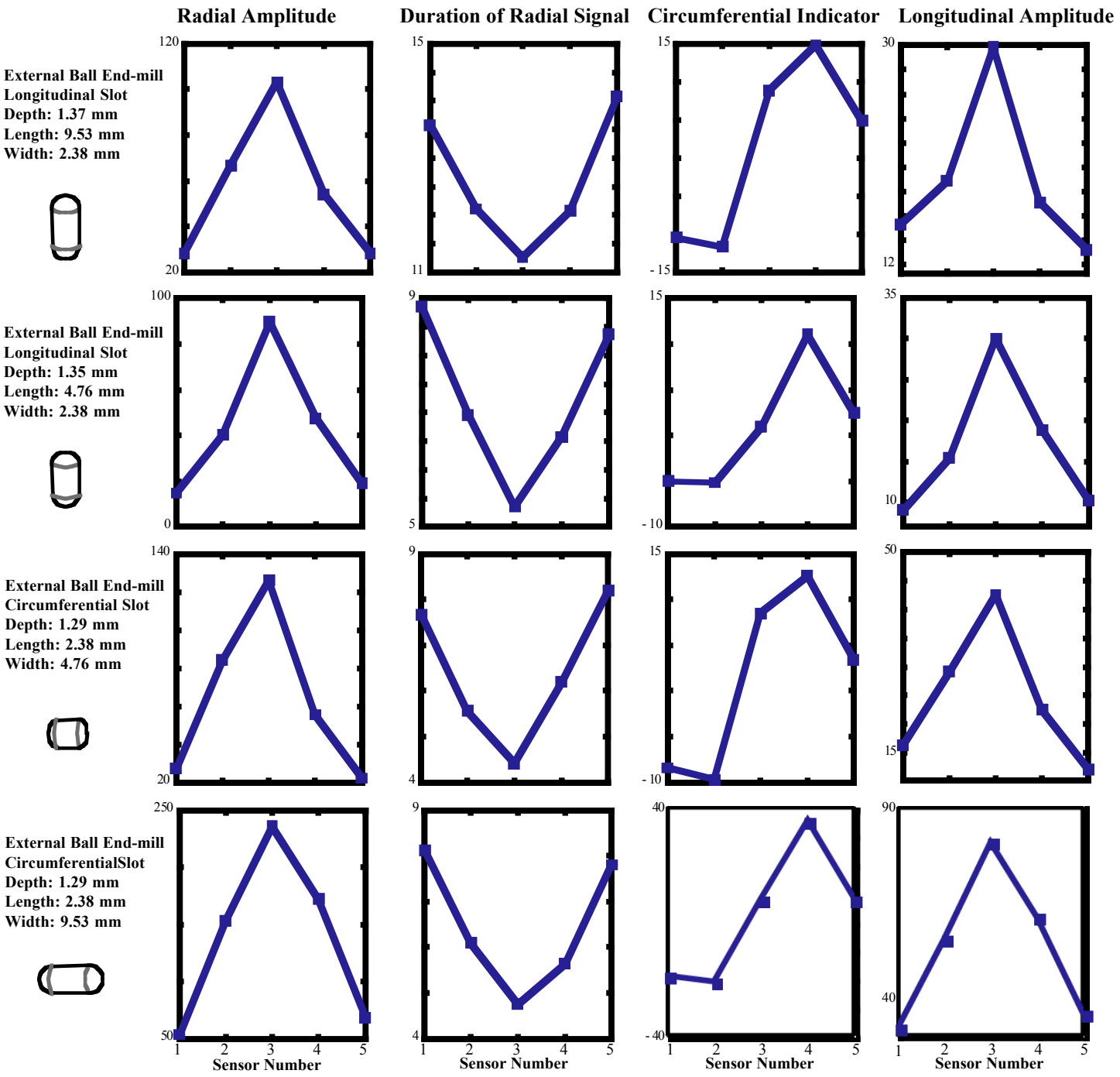
Radial Amplitude
Duration of Radial Signal
Circumferential Indicator
Longitudinal Amplitude
External Ball End-mill
Longitudinal Slot
Depth: 1.37 mm
Length: 9.53 mm
Width: 2.38 mm
External Ball End-mill
Longitudinal Slot
Depth: 1.35 mm
Length: 4.76 mm
Width: 2.38 mm
External Ball End-mill
Circumferential Slot
Depth: 1.29 mm
Length: 2.38 mm
Width: 4.76 mm
External Ball End-mill
CircumferentialSlot
Depth: 1.29 mm
Length: 2.38 mm
Width: 9.53 mm
Sensor Number

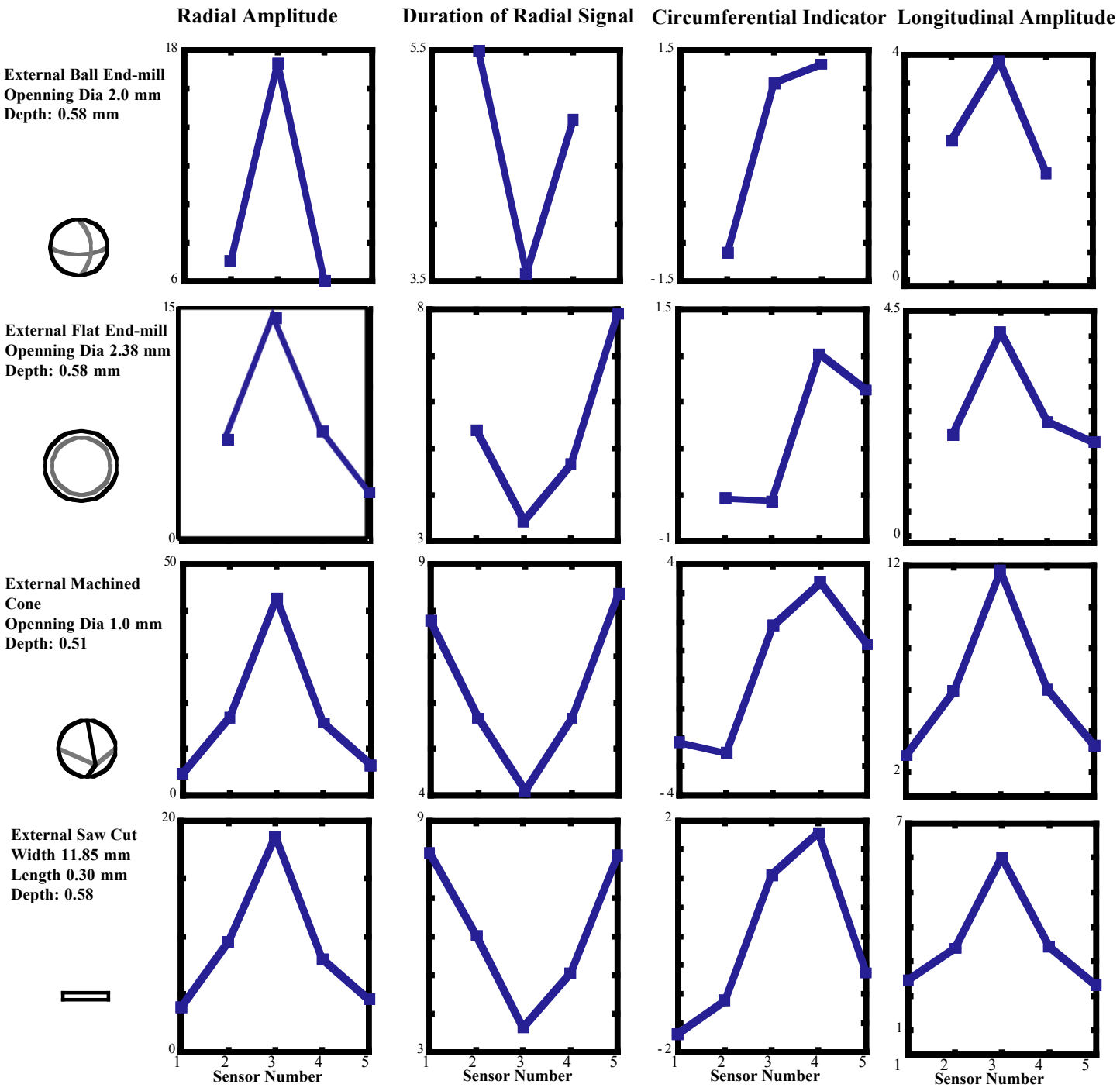
Radial Amplitude
Duration of Radial Signal
Circumferential Indicator
Longitudinal Amplitude
External Ball End-mill
Openning Dia 2.0 mm
Depth: 0.58 mm
External Flat End-mill
Openning Dia 2.38 mm
Depth: 0.58 mm
External Machined
Cone
Openning Dia 1.0 mm
Depth: 0.51
External Saw Cut
Width 11.85 mm
Length 0.30 mm
Depth: 0.58
18
6
5.5
3.5
1.5
-1.5
4
0
15
0
8
3
1.5
-1
4.5
0
50
0
9
4
4
-4
12
2
20
0
9
3
2
-2
7
1
1 2 3 4 5
Sensor Number

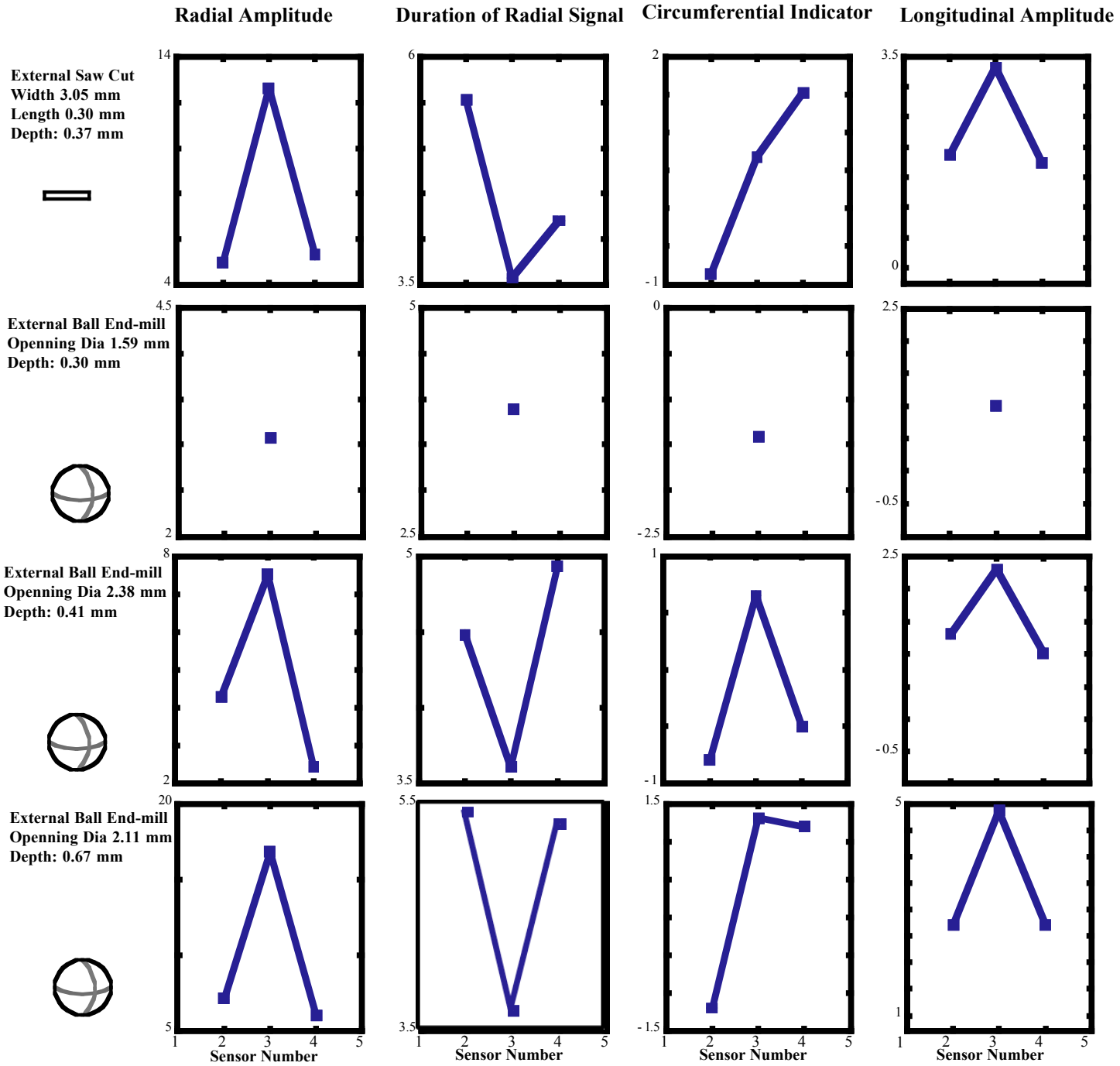
Radial Amplitude
Duration of Radial Signal
Circumferential Indicator
Longitudinal Amplitude
External Saw Cut
Width 3.05 mm
Length 0.30 mm
Depth: 0.37 mm
External Ball End-mill
Openning Dia 1.59 mm
Depth: 0.30 mm
External Ball End-mill
Openning Dia 2.38 mm
Depth: 0.41 mm
External Ball End-mill
Openning Dia 2.11 mm
Depth: 0.67 mm
Sensor Number

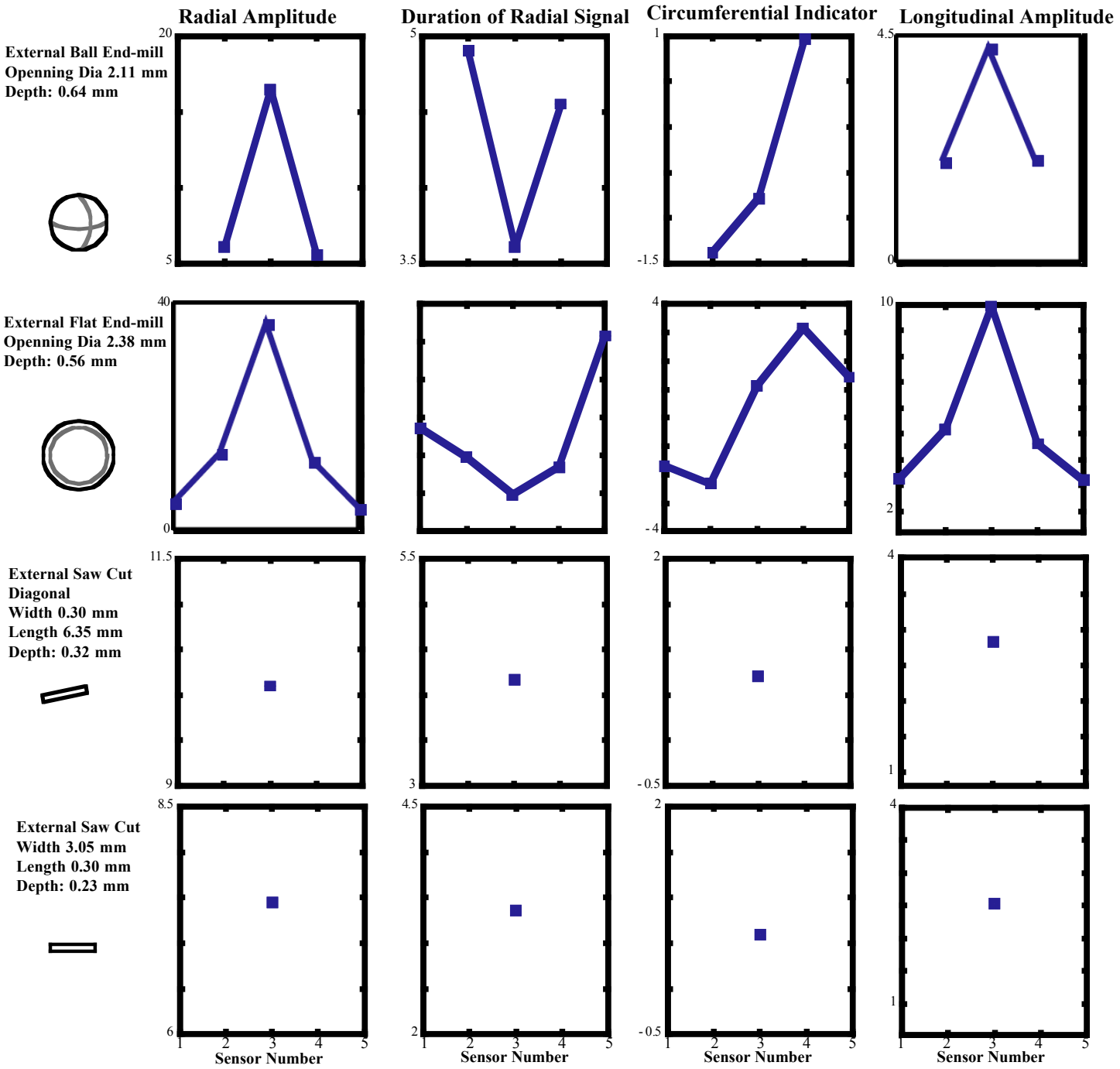
Radial Amplitude
Duration of Radial Signal
Circumferential Indicator
Longitudinal Amplitude
External Ball End-mill
Openning Dia 2.11 mm
Depth: 0.64 mm
External Flat End-mill
Openning Dia 2.38 mm
Depth: 0.56 mm
External Saw Cut
Diagonal
Width 0.30 mm
Length 6.35 mm
Depth: 0.32 mm
External Saw Cut
Width 3.05 mm
Length 0.30 mm
Depth: 0.23 mm
Sensor Number

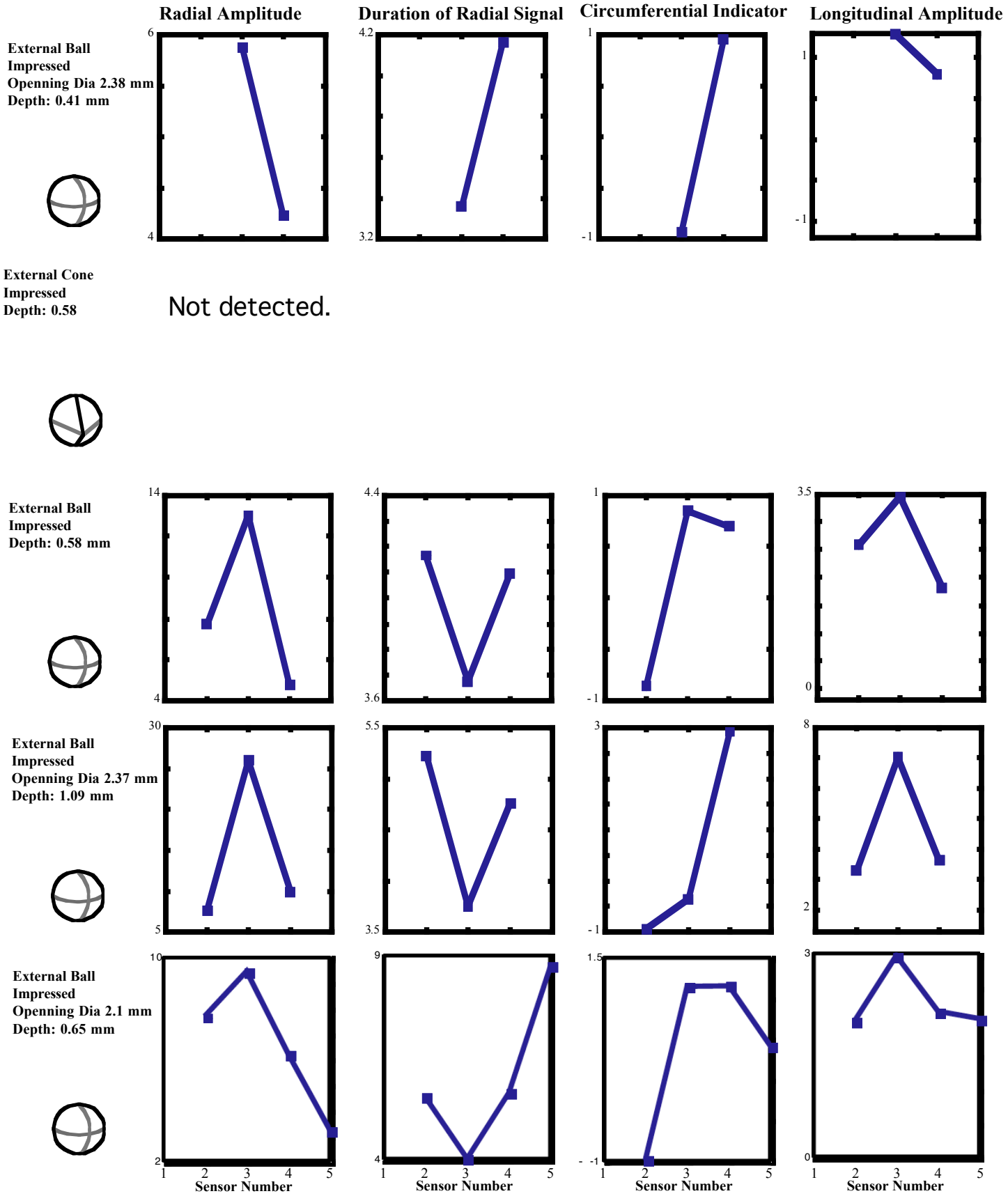
Radial Amplitude
Duration of Radial Signal
Circumferential Indicator
Longitudinal Amplitude
External Ball Impressed Openning Dia 2.38 mm Depth: 0.41 mm
External Cone Impressed Depth: 0.58
Not detected.
External Ball Impressed Depth: 0.58 mm
External Ball Impressed Openning Dia 2.37 mm Depth: 1.09 mm
External Ball Impressed Openning Dia 2.1 mm Depth: 0.65 mm
Sensor Number

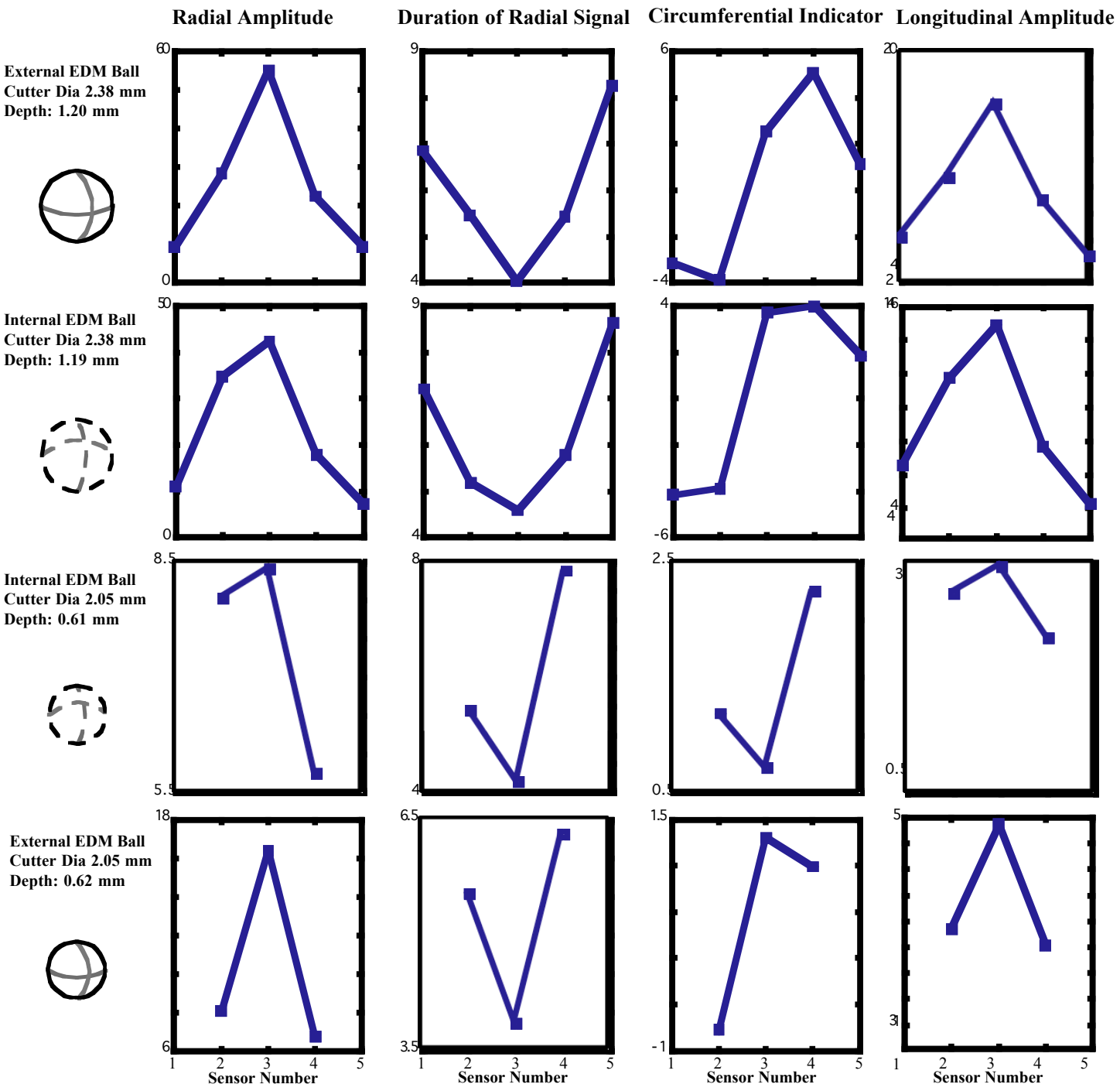
Radial Amplitude
Duration of Radial Signal
Circumferential Indicator
Longitudinal Amplitude
External EDM Ball
Cutter Dia 2.38 mm
Depth: 1.20 mm
Internal EDM Ball
Cutter Dia 2.38 mm
Depth: 1.19 mm
Internal EDM Ball
Cutter Dia 2.05 mm
Depth: 0.61 mm
External EDM Ball
Cutter Dia 2.05 mm
Depth: 0.62 mm
Sensor Number

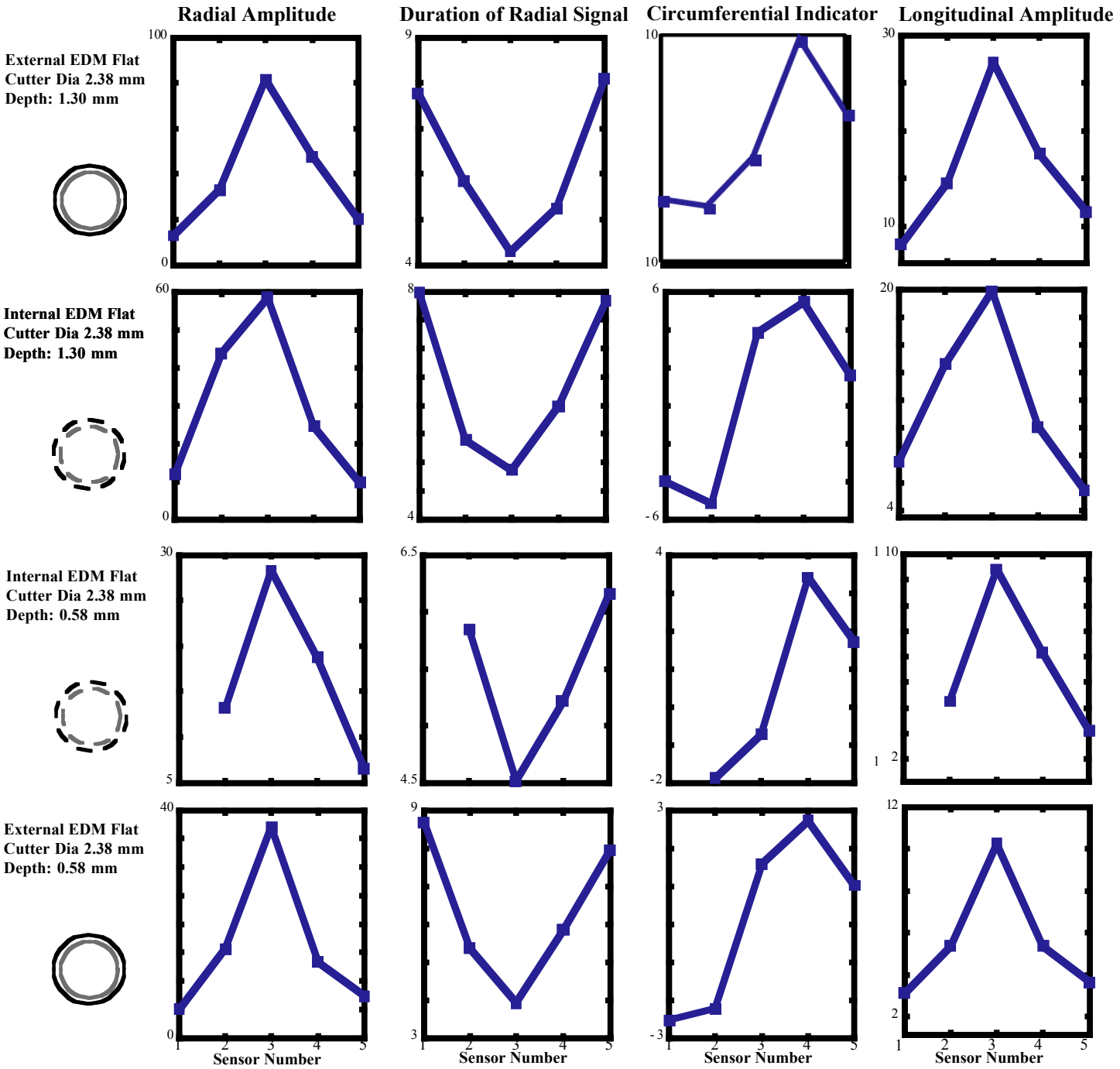
Radial Amplitude
Duration of Radial Signal
Circumferential Indicator
Longitudinal Amplitude
External EDM Flat
Cutter Dia 2.38 mm
Depth: 1.30 mm
Internal EDM Flat
Cutter Dia 2.38 mm
Depth: 1.30 mm
Internal EDM Flat
Cutter Dia 2.38 mm
Depth: 0.58 mm
External EDM Flat
Cutter Dia 2.38 mm
Depth: 0.58 mm
Sensor Number

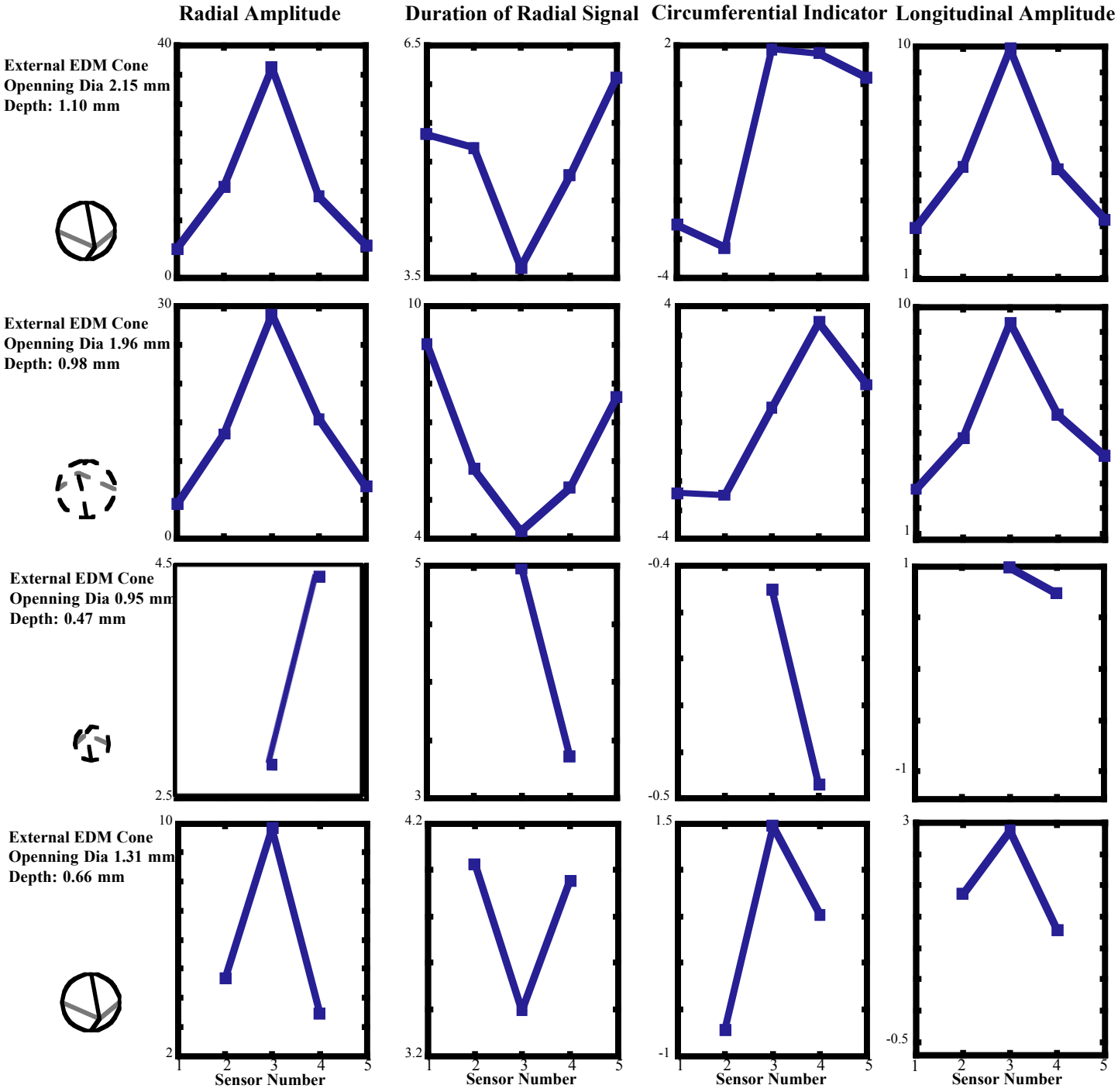
Radial Amplitude
Duration of Radial Signal
Circumferential Indicator
Longitudinal Amplitude
External EDM Cone
Openning Dia 2.15 mm
Depth: 1.10 mm
External EDM Cone
Openning Dia 1.96 mm
Depth: 0.98 mm
External EDM Cone
Openning Dia 0.95 mm
Depth: 0.47 mm
External EDM Cone
Openning Dia 1.31 mm
Depth: 0.66 mm
Sensor Number

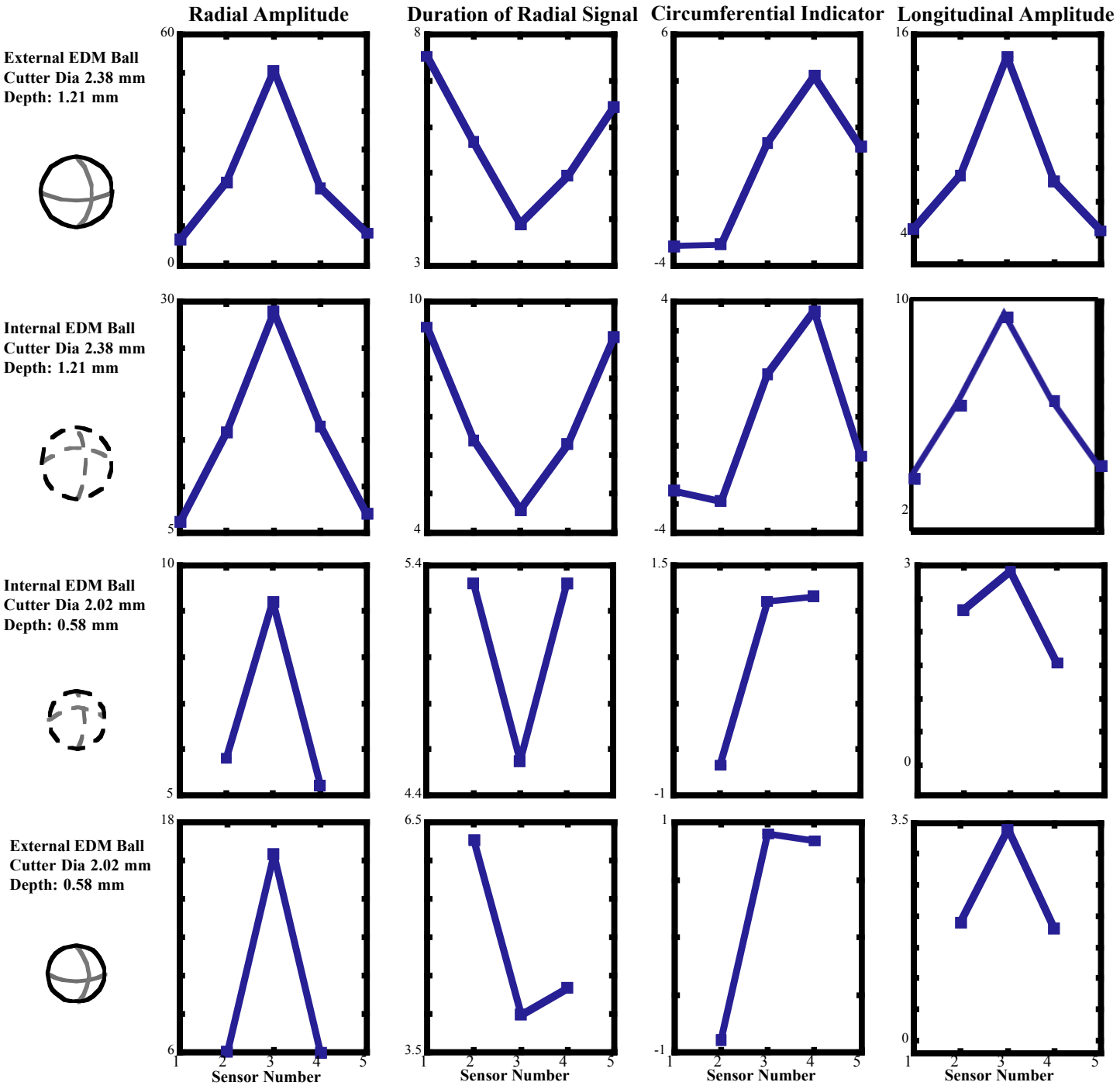
Radial Amplitude
Duration of Radial Signal
Circumferential Indicator
Longitudinal Amplitude
External EDM Ball
Cutter Dia 2.38 mm
Depth: 1.21 mm
Internal EDM Ball
Cutter Dia 2.38 mm
Depth: 1.21 mm
Internal EDM Ball
Cutter Dia 2.02 mm
Depth: 0.58 mm
External EDM Ball
Cutter Dia 2.02 mm
Depth: 0.58 mm
Sensor Number

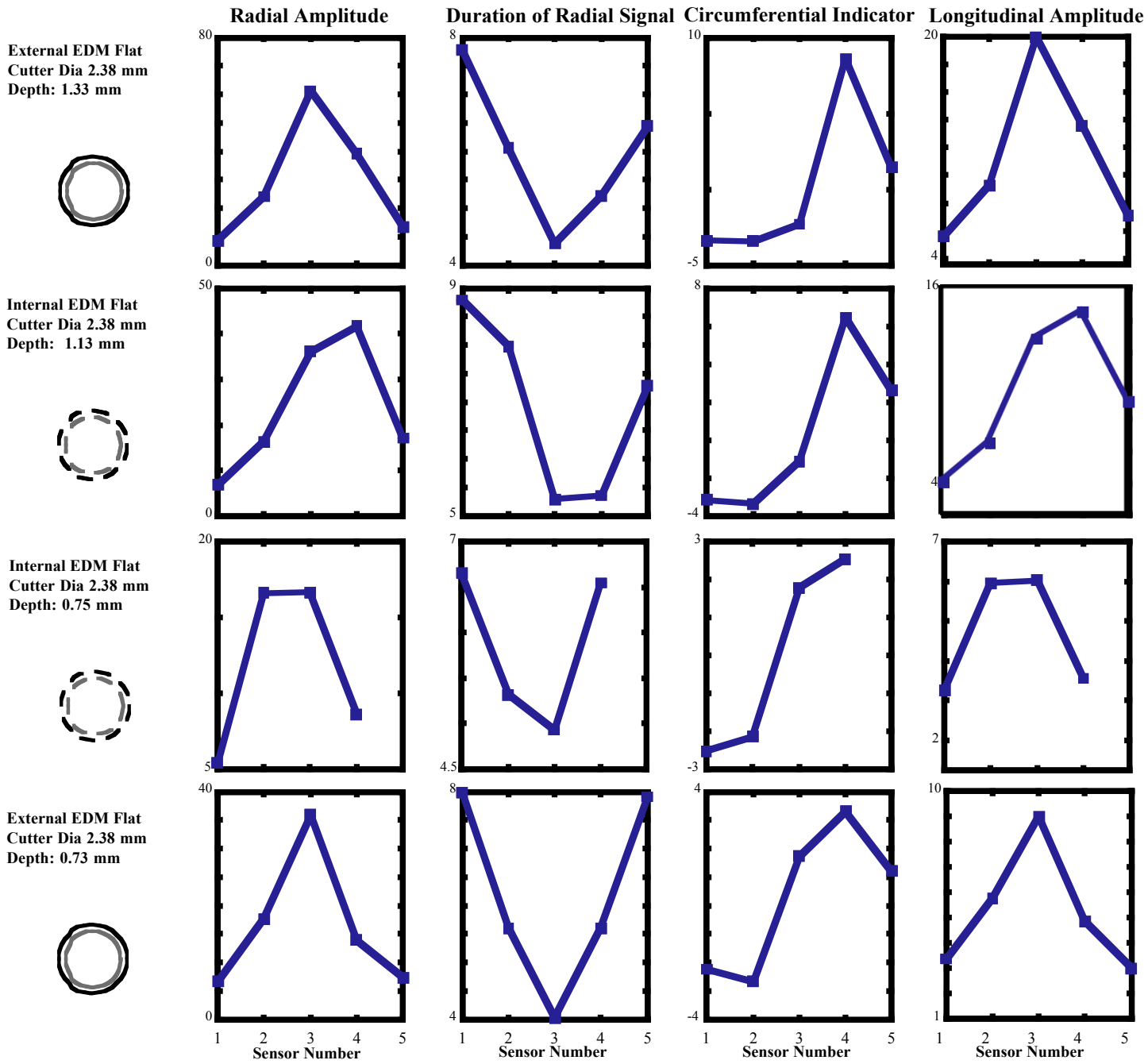
Radial Amplitude
Duration of Radial Signal
Circumferential Indicator
Longitudinal Amplitude
External EDM Flat
Cutter Dia 2.38 mm
Depth: 1.33 mm
Internal EDM Flat
Cutter Dia 2.38 mm
Depth: 1.13 mm
Internal EDM Flat
Cutter Dia 2.38 mm
Depth: 0.75 mm
External EDM Flat
Cutter Dia 2.38 mm
Depth: 0.73 mm
80
0
8
4
10
-5
20
4
50
0
9
5
8
-4
16
4
20
5
7
4.5
3
-3
7
2
40
0
8
4
4
-4
10
1
1 2 3 4 5
Sensor Number

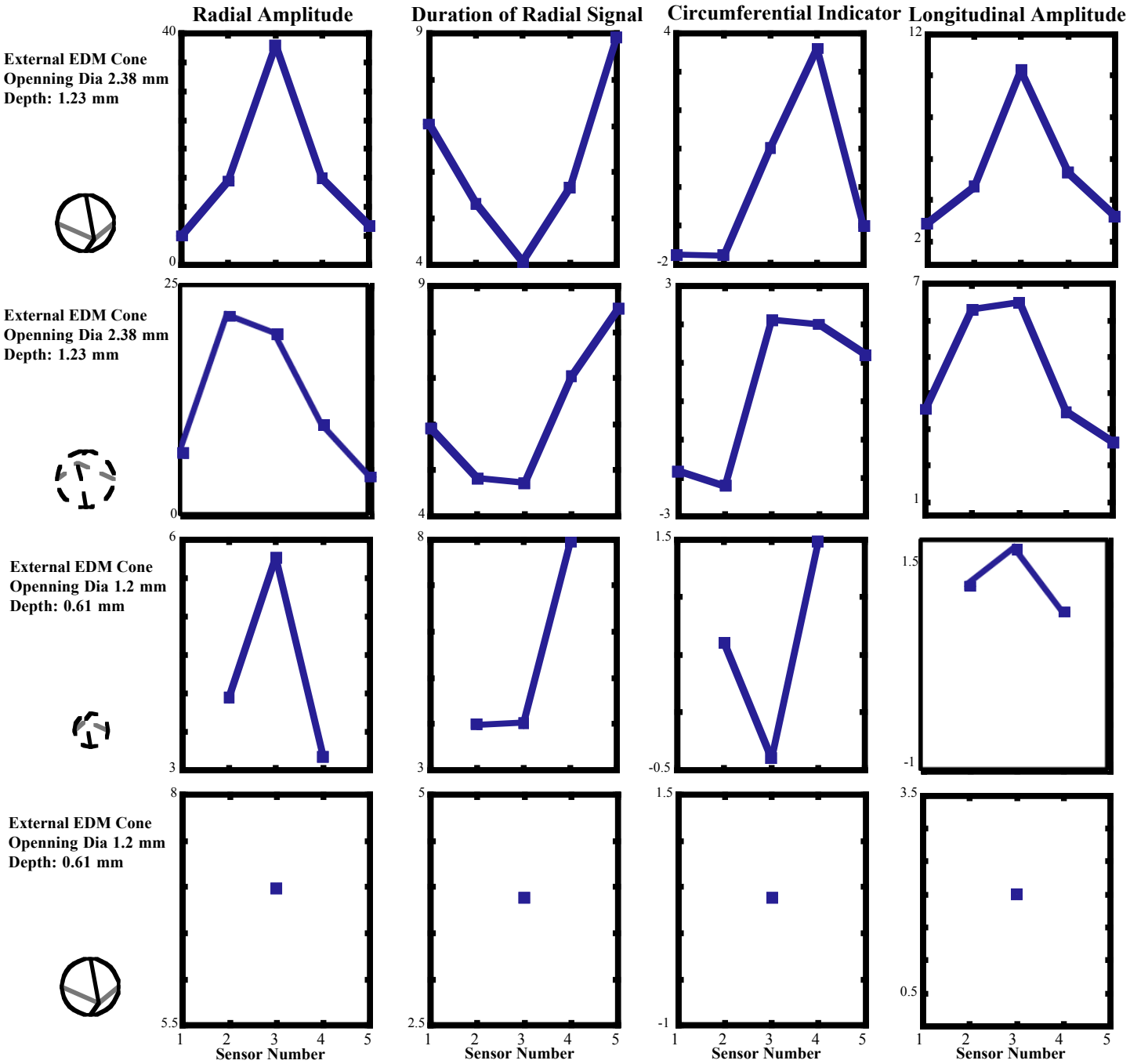
Radial Amplitude
Duration of Radial Signal
Circumferential Indicator
Longitudinal Amplitude
External EDM Cone
Openning Dia 2.38 mm
Depth: 1.23 mm
External EDM Cone
Openning Dia 2.38 mm
Depth: 1.23 mm
External EDM Cone
Openning Dia 1.2 mm
Depth: 0.61 mm
External EDM Cone
Openning Dia 1.2 mm
Depth: 0.61 mm
Sensor Number
Sensor Number
Sensor Number
Sensor Number

Detection of Coiled Tubing Defects Using Matched Filter Algorithm

T. R. McJunkin *, K. S. Miller, C. R. Tolle, A. D. Watkins, E. D. Larsen

Idaho National Laboratory, P.O. Box 1625, Idaho Falls, ID 83415-2210 USA

Abstract

Coiled tubing is commonly used in the oil industry for servicing wells. This article describes a new method for defect detection using magnetic flux leakage inspection of coiled tubing. A highly efficient defect detection method has been developed using a matched filter, derived from general flaw signal characteristics. The matched filter has been optimized and validated based on a library of signals acquired from a diverse set of artificial flaws inserted into coiled tubing developed in conjunction with the University of Tulsa. Effects of sensor liftoff and detection of liftoff are also discussed.

Key words: Flux leakage; Coiled tubing; Matched filters; Defect detection

1 Introduction

Over the last several decades, the use of coiled tubing (CT) for servicing wells in oil fields has significantly increased as operators capitalized on the economic benefits of its use and reuse [1]. At the same time, the reliability of current CT products has increased markedly due to improvements in equipment, operating procedures, and the tube manufacturing process. Current oil field CT use involves running a continuous string of CT into a well to perform specific operations, e.g. pumping, acidizing, or electronic measurement instrument logging, without disturbing existing equipment in the well. When servicing is complete, the CT is withdrawn onto a large spool for transport to the next work location or storage. Even though CT reliability has increased, the potential cost of any failure, in terms of safety and loss of well production, remains quite high; therefore, efforts to increase reliability are continuing [2, 3].

* Corresponding author. Tel.: +1-208-526-7895; fax: +1-208-526-0690.
Email address: `timothy.mcjunkin@inl.gov` (T. R. McJunkin).

Reliability issues arise from several sources: wear (surface, fatigue, and corrosion damage); material and manufacturing defects; and operator error. The major factor affecting CT life is fatigue [4, 5] due to severe bending strains that exceed CT material yield strengths. CT string vitality has been evaluated using cumulative bending cycle counts. These counts, along with pressure, geometry, and material properties, are input into sophisticated plasticity and fatigue damage models to predict the extended service life for discrete sections of CT along the string. However, in the field CT can fail sooner than these models predict. This is, in part, due to the presence of unknown defects from surface damage and/or corrosion during field use, that fatigue models do not take into account [5]. Accurately incorporating flaw data into fatigue models would greatly improve their failure prediction capability.

Various CT field inspection technology are used to nondestructively obtain flaw information from CT, including rolling friction wheels to monitor depth, diameter, and ovality. Magnetic flux leakage systems are used to identify defects in some inspection systems. Most of the magnetic flux leakage systems consolidate data signals to an average of all sensors to simplify evaluation of inspection signals. This compression directly leads to low reliability in identifying the type of defect present (cracks, corrosion, etc.) as well as in dimensional information for most defects detected . Reliable analysis of magnetic flux leakage is also hampered by intrinsically noisy signals, due to mechanical chatter. A standard band-pass filter and signal amplitude threshold approach is not effective at detecting small defects.

This article presents a highly effective automatic flaw detection technique, based on a matched filter optimized for the magnetic flux leakage data. The results presented are based on a library of 66 defects. Additionally, the results of a study of the effects of sensor liftoff are discussed. We also provide recommendations for signal detection, sensor head design, and characterization algorithms. A final goal of this work is the merger of an automatic flaw detection and characterization system with the lifetime prediction model [5] being developed by the University of Tulsa.

2 Equipment overview

A laboratory scale experimental CT magnetic flux leakage sensor head has been constructed, see Fig. 1. All of the data presented within this article was acquired using this device.

The magnetic flux for the sensor is produced by a coil surrounding the magnetic sensors and the pipe. The coil is 89 mm long with an inner diameter of 102 mm. It consists of 1400 revolutions (turns) of an 18 gauge copper wire insulated with a

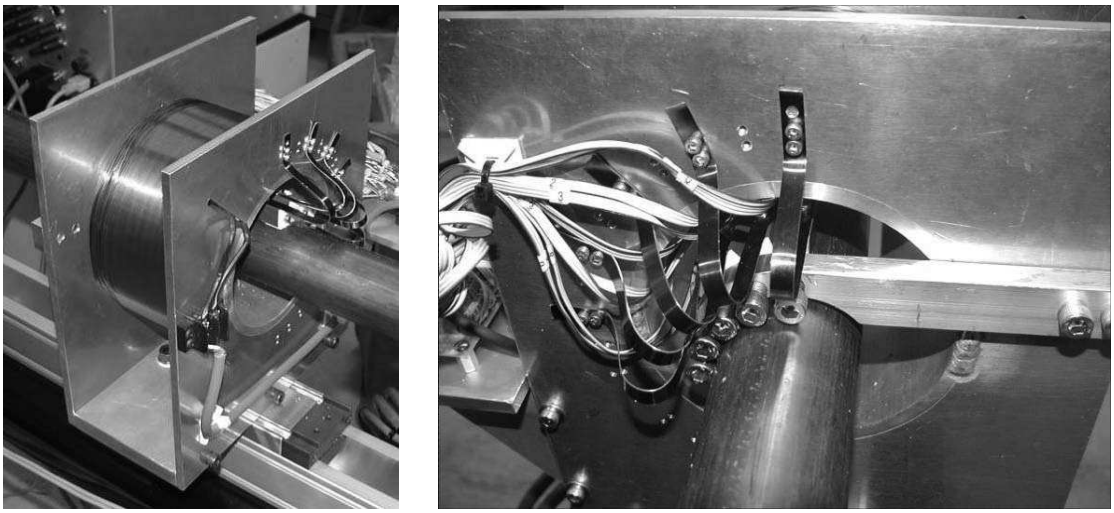

Fig. 1. INL's coiled tubing flaw detection sensor head (left), and an end view close-up of the Hall-effect sensor packages (right).

lacquer finish. A current-controlled power supply (Xantrex XHR 100-10DC) supplies up to 7 A of direct current to the coil. The magnetic field is proportional to the number of turns and the amplitude of the current. A higher current allows better sensitivity to flaws; however, while maintaining a current of 7 A, the coil temperature rises beyond the desirable operating range in a short period of time. Nevertheless, for the defects in this study, the system can be run using lower current levels without loss of detection ability.

Ratiometric linear Hall-effect sensors (Allegro Microsystems A3518SUA) are housed in a spring loaded plastic frame with delrin shoes that ride on the surface of the tubing. This wearable shoe differs from many coiled tubing sensors that use a fixed standoff for the sensors. Most existing industry sensor packages contain only two orthogonal components of the magnetic field (radial and longitudinal). A third sensor for measuring the circumferential component is included in our system.

For the experiments described below, five shoes were distributed around approximately one quarter of the circumference of a tube. The shoes were spaced about 22.5 degrees apart. Tubes with known defects were measured with the flaw centered on the middle of the five shoes, thereby allowing measurement of the magnetic field over one fourth of the tubing circumference. For field use, additional sensors would be added to encompass the entire circumference.

For experimental convenience, the magnetic coil and sensors are moved while the CT sample remains stationary. The magnetic coil and sensors are attached to a linear slide (Parker Daedal Belt drive actuator model HLE RB). The linear slide has a travel of 1.52 m and is powered by a Parker Compumotor

OS stepper motor (OS22B-SNL10) with a 10:1 actuator gear box. The motor is controlled using a Zeta 6104 Parker Compumotor stepper drive/controller. The experiment is controlled by a Labview (National Instruments) program executed on a computer workstation (Dell Computer Corporation), which interfaces to the motor controller though an RS-232 serial port. A specified constant velocity, excluding the duration of acceleration at the beginning and end of a run, was achieved by controlling the stepping frequency of the motor. Because data was acquired at a fixed sampling rate, data during the accelerations was excluded from analysis. Hall effect sensor data was acquired with a National Instruments digital acquisition card (Model 6062E) with a sampling rate of 2000 samples/s on each sensor. The raw data signals were pre-processed for noise reduction using a first-order low pass Butterworth filter with a cutoff frequency of 100 Hz.

3 Matched filter algorithm

The flaw detection problem in CT is similar to that of other detection problems, e.g. the radar problem [6], in that the signal of interest is embedded in noise due to the environment of the application. In the radar problem, it may be possible to signal average over repetitive samples. However, in CT flaw detection this is not an option because the signal is produced by the motion of the CT through the sensor. Another approach used in the radar problem is to correlate the known signal *shape* with the received signal. The general shape of a flaw signature can be found from large, easily-detected flaws. Using a distinctive signature, a matched filter [6, 7] is implemented with a correlation of the filter transform $h(t)$ with the signal $s(t)$,

$$\nu(t) = \int_{-\infty}^{\infty} s(\tau)h(\tau - t)d\tau, \qquad (1)$$

that produces a maximum response to the signal of interest while rejecting noise. For CT, the signal shape of the radial component of the magnetic flux leakage is very distinctive. This component, in response to a circular hole, produces a signal with respect to longitudinal position of the sensor that is an odd function, $f(t) = -f(-t)$, when the possible constant offset is removed. This signature takes the form of a positive pulse followed by a negative pulse, as shown in Fig. 2. Furthermore, this signature approximates the first derivative of a Gaussian:

$$\frac{d}{dt}e^{-(t/t_o)^2} = -\frac{2t}{t_o}e^{-(t/t_o)^2}, \qquad (2)$$

which has a maximum at $t_{max} = -\frac{t_o\sqrt{2}}{2}$ and a minimum at $t_{min} = \frac{t_o\sqrt{2}}{2}$ at the finite values of t for roots of the second derivative of the Gaussian,

$$\frac{d^2}{dt^2}e^{-(t/t_o)^2} = \frac{2}{{t_o}^2}e^{-(t/t_o)^2}\left[\frac{2t^2}{{t_o}^2} - 1\right] = 0. \qquad (3)$$

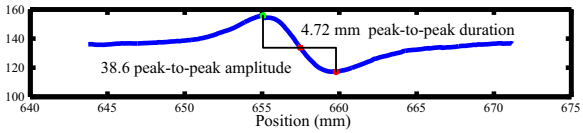

Fig. 2. The radial component response to a 0.81 mm deep round-bottom hole made using a 2.38 mm diameter bit. The diameter of the opening of the hole is approximately 2.26 mm.

The duration in time between maximum peak and minimum peak of the radial component response is dependent on size, i.e. primarily the longitudinal length of the defect, and therefore the velocity, υ, at which the sensor is passing over the tubing. The data is normalized by converting the free variable from time, t, to position, l, (i.e $l = \upsilon t$ and $l_o = \upsilon t_o$). For a constant size defect, a matched filter with the shape of the derivative of the Gaussian seems to be a reasonable choice for our detection filter. With no a priori knowledge of the size of flaws to be detected, the width of such a filter remains difficult to optimize; however, detection capability for larger flaws is maintained when optimizing for smaller flaws. Choosing a peak-to-peak length, the filter becomes:

$$h(l) = -\frac{2l}{l_o} e^{-(l/l_o)^2}, \qquad (4)$$

$$\text{where } l_o = \frac{l_d\sqrt{2}}{2}.$$

Since the signal is to be digitized, the filter can be rewritten as:

$$h(n) = -\frac{2\upsilon T n}{l_o} e^{-(\upsilon T n/l_o)^2} \qquad (5)$$

$$= -2\kappa n e^{-(\kappa n)^2} \qquad (6)$$

$$\text{where } \kappa = \frac{\upsilon T}{l_o}$$

$$\text{or } \kappa = \frac{\upsilon T\sqrt{2}}{l_d},$$

where n is the sample number and T is the sample period. For practical use, the filter is truncated to a reasonable range. We choose the range to be equivalent to $2l_d$ or all integers i in the range $\left[-round\left(\frac{l_d}{\upsilon T}\right), round\left(\frac{l_d}{\upsilon T}\right)\right]$. The digitized filter in terms of sample numbers is:

$$\nu(n) = \sum_{i'=n-L}^{n+L} s(i')h(i'-n), \qquad (7)$$

letting $L = round\left(\frac{l_d}{\upsilon T}\right)$. By shifting the summation with $i' = i + n$, eq. (7) becomes simply:

$$\nu(n) = \sum_{i=-L}^{L} s(i+n)h(i), \qquad (8)$$

where $s(n)$ is the digitized signal, $s(t)$. The non-causal filter requires a delay of L samples to implement in real time.

The output of this matched filter forms the basis for detection of a defect. A threshold for flaw detection was initially heuristically chosen by examining the matched filter results for standard defects manufactured into new coiled tubing samples. A threshold level, combined with the width of a resultant signal $\nu(n)$, has proven quite effective. The width of the signal is measured between the zero crossings of $\nu(n)$ before and

after the threshold crossing. The minimum zero-crossing width was chosen to be slightly shorter than the zero-crossing width of the autocorrelation of the filter signal.

To simplify the computations further, a two-point representation of the filter was considered. Namely, the positive and negative peaks separated by a fixed position displacement distance located at extremes of the original filter signal. The simplified filter is written as:

$$h_s(l) = a\left[\delta(\frac{l_d}{2} - l) - \delta(\frac{l_d}{2} + l)\right], \quad (9)$$

where δ is the unit impulse function. The discrete form as a function of sample number, n, is:

$$h_s(n) = a\left[\delta(n_d - n) - \delta(n_d + n)\right], \quad (10)$$

where $n_d = round(\frac{l_d}{2Tv})$ and a is a scaling factor. The resulting correlation with the signal, $s(n)$, is:

$$\nu_s(n) = a\left[s(n - n_d) - s(n + n_d)\right]. \quad (11)$$

To allow the filters to be compared directly, the appropriate adjustment of $h_s(n)$ is found by finding the scaling factor a in $h_s(n)$ to make the correlation of h_s with h at $n = 0$ to be equal to the autocorrelation of h_s at $n = 0$:

$$\sum_{i=-L}^{L} h(i)^2 = \sum_{i=-L}^{L} h(i)h_s(i) \quad (12)$$
$$= a\left[h(-n_d) - h(n_d)\right].$$

The scale factor is:

$$a = \frac{\sum_{i=-L}^{L} h(i)^2}{h(-n_d) - h(n_d)} \quad (13)$$
$$= \frac{\sum_{i=-L}^{L} h(i)^2}{2h(-n_d)}. \quad (14)$$

A comparison of the two filters was completed on the same data set taken from a pipe with regularly-shaped defects of various sizes inserted into coiled tubing. Both flat-bottom (FB) and round-bottom (RB) mill bits were used in machining these flaws. The details and flaw number assignment of the targets in this pipe section, designated CT1, are given in Table 1. Both filters produce an output that is normalized to zero baseline to allow for a simple constant amplitude detection threshold. In Figs. 3 and 4, the noise in the two-point filter is substantially higher than that of the full Gaussian filter. The smoothing effect of the Gaussian filter has the benefit of further rejecting high frequency noise due to mechanical chatter during a scan. A threshold can reliably be set to a lower amplitude and still be above the background noise. More noise passes through the simpler filter and produces false detections if the threshold is set low enough to detect the simulated flaw with the smallest amplitude signal in CT1, see Flaw 4 in Fig. 3.

Fig 5. shows the result of applying the full Gaussian to a raw data set. The output is filtered nearly as well as when applied after the Butterworth filter shown in the previous examples, Figs. 3 and 4. These results support our

Table 1
Physical geometry and the detected signal amplitudes and durations of artificial flaws in CT1.

Flaw Parameters						Detection Values	
Tube Name	Flaw No.	Type	Cutter Dia. (mm)	Depth (mm)	Opening Dia. (mm)	Radial Amplitude	Radial Duration(mm)
CT1	1	RB	4.76	1.58	4.48	51.8	4.4
CT1	2	RB	4.76	1.07	3.97	34.2	4.5
CT1	3	RB	4.76	0.81	3.58	19.8	4.1
CT1	4	RB	4.76	0.38	2.58	5.2	3.5
CT1	5	FB	4.76	1.58	4.76	79.9	4.5
CT1	6	FB	4.76	1.17	4.76	57.5	4.4
CT1	7	FB	4.76	0.79	4.76	40.4	4.0
CT1	8	FB	4.76	0.38	4.76	18.3	4.0

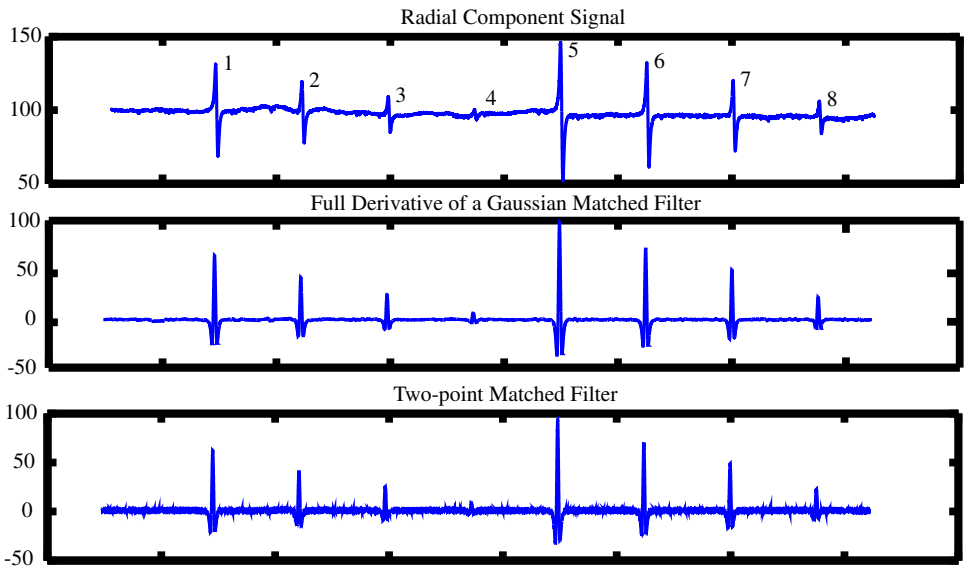

Fig. 3. Results for two matched filters for sample CT1, containing a series of eight known defects, see Table 1. The top signal shows the acquired radial sensor signal. The middle signal is the result of a full Gaussian derivative matched filter. The bottom signal shows the result of a two-point matched filter.

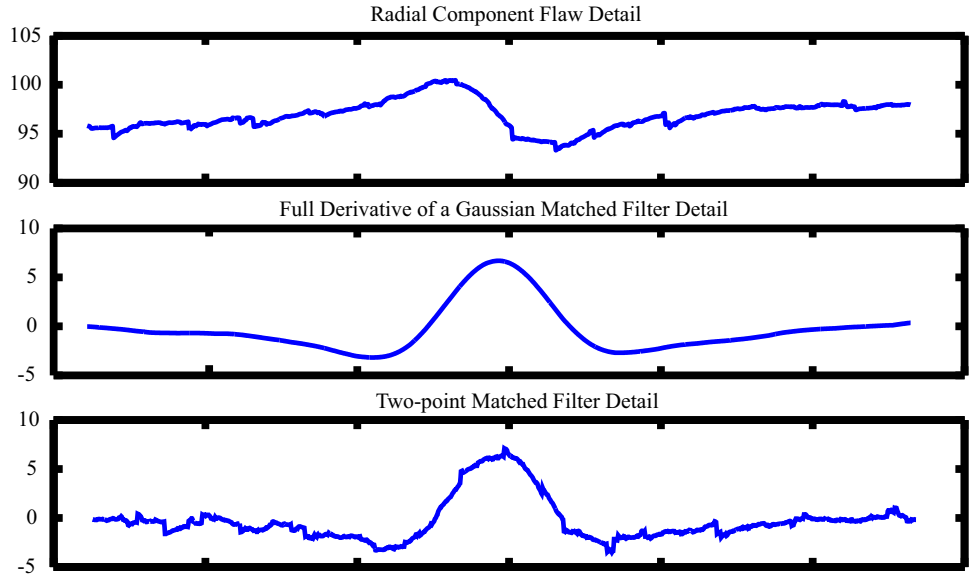

Fig. 4. Results for two matched filters on Flaw No. 4 in CT1. Top signal shows the acquired radial sensor signal. The middle signal is the result of a full Gaussian derivative. The bottom signal shows the result of a two point filter.

recommendation for the use of the full Gaussian without the low-pass Butterworth filter described in Section 2.

Data was acquired and processed on additional tubes with artificial flaws. Results for a tube with various machined FB holes and longitudinal(LSlot) and circumferential (CSlots) slots, designated CT2, are given in Table 2. Additional sets of flawed sample tubes were provided by the University of Tulsa (TU). The TU samples contain a diverse assortment of flaws created with machining, pressing, and electro-discharge machining (EDM). In addition to RB and FB holes and slots, the TU samples include saw cuts and cone-shaped flaws. A set of some types of flaws was created on both the outer and inner diameter of the pipe. Lists of flaws in TU pipes are included in Tables 3 through 6. All of the flaws in CT1, CT2, and the TU pipes were scanned to create a library of data sets to form the basis for determining appropriate thresholds and validating the detection algorithms.

An amplitude threshold of 2.5 and a minimum zero-crossing width of 4.5 mm applied to the output of the matched filter was found to be effective for a magnet current of 5 A. The length, $l_d = 3.4$ mm, was chosen heuristically based on the shortest peak-to-peak duration on CT1. With the exception of TU Flaw 22, all flaws listed in Tables 1 through 6 have been successfully detected automatically using data from tubes run at 700 mm/s travel speed and 5 A coil current. At these thresholds, a small number of false detections occurred. These false detections might be excluded by adding more

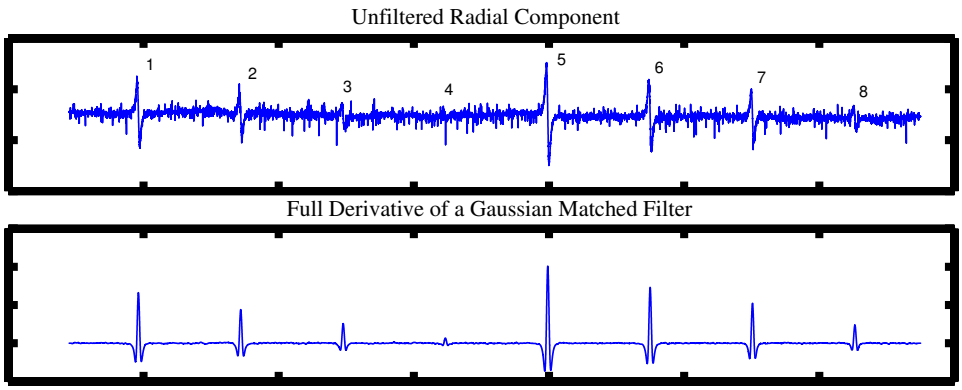

Fig. 5. The full Gaussian filter response to the raw data without Butterworth low-pass filtering.

sophisticated threshold rules to the detection algorithm. Since the false detections often occur only on one of the circumferential sensor sets and actual flaws, in general, occur on multiple adjacent sensors, a filter for detection requiring multiple sensor detections might reduce false detections. TU Flaw 22 is a cone shaped flaw that produces a very low amplitude signal. An amplitude threshold value of less than 1 that would detect this flaw would produce many more false detections.

The relative peak-to-peak amplitude and duration of the radial component were returned automatically by the analysis software that was written to implement the algorithm. Values for each detected flaw are listed in Tables 1 through 6.

4 Longitudinal component sensor for liftoff detection

The sensors were adjusted to intentionally leave space between the shoe (a.k.a. liftoff) and the tube being inspected. Liftoff is designed into some sensor packages, using a nominal standoff to avoid the issues associated with probes contacting the surface, such as pipe cleanliness. In sensor systems designed with a suspension to keep the shoes in contact with the pipe, surface conditions may cause the sensor to "bounce," causing a transient liftoff condition. The effects of liftoff were studied on several tubes.

Liftoff has a number of effects on the signature of a flaw. For example, the baseline amplitude of the longitudinal sensor signal is a function of liftoff, see Fig. 6. Unfortunately, this baseline effect is neither linear nor monotonic. Moreover, there is a rapid decrease in baseline signal strength with liftoffs of greater than 2 mm. Nevertheless, the baseline can be used as a diagnostic indicator of liftoff if a system is designed to nominally operate with near zero liftoff. The radial sensor signal is also attenuated, which is the primary reason for loss of sensitivity

Table 2
Physical geometry and the detected signal amplitudes and durations of artificial flaws in CT2.

Flaw Parameters							Detection Values	
Tube Name	Flaw No.	Type	Cutter Dia. (mm)	Long. Dim. (mm)	Circ. Dim. (mm)	Depth (mm)	Radial Amplitude	Radial Duration (mm)
CT2	1	hole	2.54	2.54	2.54	1.52	92.2	4.3
CT2	2	hole	4.76	4.76	4.76	1.52	193.1	5.7
CT2	3	hole	6.35	6.35	6.35	1.52	270.9	7.4
CT2	4	LSlot	2.38	9.55	2.38	1.52	131.4	10.0
CT2	5	LSlot	2.38	7.24	2.38	1.52	130.4	7.9
CT2	6	LSlot	2.38	4.83	2.38	1.52	116.5	5.7
CT2	7	CSlot	2.38	2.38	9.56	1.52	288.4	5.0
CT2	8	CSlot	2.38	2.38	7.13	1.52	237.4	4.9
CT2	9	CSlot	2.38	2.38	4.81	1.52	167.2	4.8

in detection due to liftoff. Fig. 7 shows a summary of the radial and longitudinal signals for a flaw with various amounts of liftoff. This illustrates other factors that adversely influence the sizing of a flaw. The duration of the radial signal is lengthened with increasing liftoff; therefore, the apparent length of the flaw is exaggerated. These effects do appear to be monotonic with respect to liftoff. Therefore, with an independent measurement of liftoff, the characterization of the flaw performed with the radial signal might be corrected. However, there is no compensation possible for the loss in detection sensitivity. Note: with zero or constant liftoff, the measured field with this sensor is proportional to the field strength and could be used as a diagnostic for appropriate current through the magnetic coil.

The effects found in this study show that liftoff should be minimized. Liftoff beyond that provide for in the contact shoe should be avoided in design of sensor heads.

5 Conclusion

This article described the effective use of a matched filter designed for the signature of the radial component of a magnetic flux leakage flaw detection system, namely the derivative of a Gaussian shape with length chosen appropriately. The filter performs very well even when the signal has not previously been filtered by a traditional low-pass filter. Detection and filtering are, therefore, possible with a single correlation. A simpler

Table 3
Geometry, method, and the detected signal amplitudes and durations of artificial flaws in TU flaws 1-13.

Flaw Parameters							Detection Values	
Flaw No.	Location	Shape	Method	Long. Dim. (mm)	Circ. Dim. (mm)	Depth Dim. (mm)	Radial Amplitude	Radial Duration (mm)
1	external	RB	machined	10.56	2.11	0.66	43.3	9.8
2	external	RB	machined	4.11	2.05	0.61	21.1	5.6
3	external	RB	machined	2.06	4.11	0.59	31.9	4.5
4	external	RB	machined	2.15	8.62	0.68	85.5	4.3
5	external	RB	machined	9.53	2.38	1.37	103.3	11.3
6	external	RB	machined	4.76	2.38	1.35	89.8	5.4
7	external	RB	machined	2.38	4.76	1.29	126.1	4.4
8	external	RB	machined	2.38	9.53	1.29	235.9	4.8
9	external	RB	machined	2.05	2.02	0.58	17.3	3.6
10	external	FB	machined	2.38	2.38	0.57	25.5	4.7
11	external	cone	machined	1.02	1.00	0.51	42.6	4.1
12	external	cut	saw	0.30	11.85	0.80	18.6	3.6
13	external	cut	saw	0.30	3.05	0.37	12.6	3.6

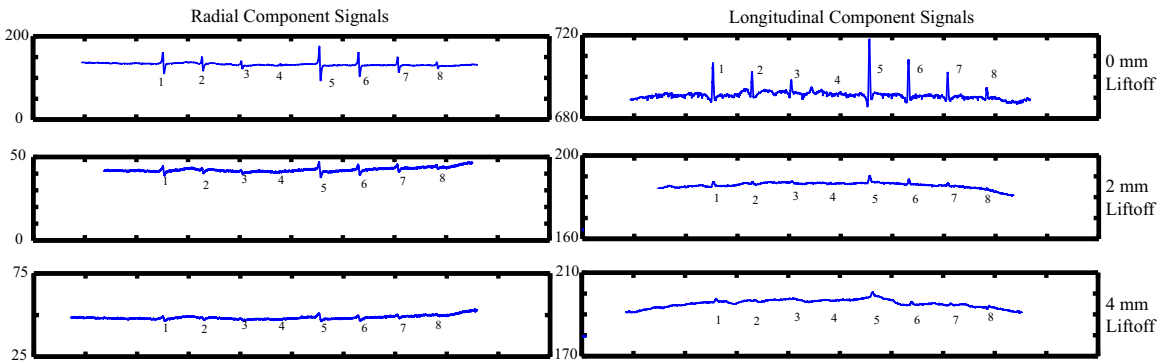

Fig. 6. This figure shows the effects of 0 mm, 2 mm, and 4 mm liftoff on the radial and longitudinal signals. The sensor shoes were set to a series of fixed radial offsets from the surface of the tubing on CT1.

Table 4
Geometry, method, and the detected signal amplitudes and durations of artificial flaws in TU flaws 14-25.

Flaw Parameters							Detection Values	
Flaw No.	Location	Shape	Method	Long. Dim. (mm)	Circ. Dim. (mm)	Depth Dim. (mm)	Radial Amplitude	Radial Duration (mm)
14	external	RB	machined	1.59	ball	0.30	3.1	3.9
15	external	RB	machined	2.38	ball	0.41	7.5	3.6
16	external	RB	machined	2.14	2.11	0.67	16.8	3.7
17	external	RB	machined	2.11	2.08	0.64	16.4	3.6
18	external	FB	machined	2.38	2.38	0.56	36.3	4.0
19	external	cut (diagonal)	saw	6.35	9.52	0.32	10.1	4.2
20	external	cut	saw	0.30	3.05	0.23	7.5	3.4
21	external	RB	impressed	2.38	ball	0.41	5.9	3.4
22	external	cone	impressed			0.58	not detected	
23	external	RB	impressed			0.58	13.0	3.7
24	external	RB	impressed	2.37	2.37	1.09	26.9	3.8
25	external	RB	impressed	2.12	2.09	0.65	9.4	4.0

two-point approximation of the filter was examined also, with reasonably good results though with more noise than the full Gaussian. The results support our recommendation to use the full derivative of a Gaussian for the detection filter.

Now that flaws are readily detected, the data from all the sensors in proximity to the flaw can be analyzed to characterize flaws. Trained neural network methods used by others [8, 9] and direct data abstraction methods in development by the authors can be applied to approximate the geometry of the flaw. Data and abstracted characteristics of the data will be applied as input to longevity predictive models [5].

The effects of liftoff of the sensor from the surface of the pipe were also illustrated. Liftoff affects sensitivity and other signal characteristics. Liftoff can be detected, but not measured, with the longitudinal component sensor. An independent measure of the liftoff might allow compensation for some signal measurement but cannot compensate for loss of signal. This result leads to a recommendation

Table 5
Geometry, method, and the detected signal amplitudes and durations of artificial flaws in TU flaws 26-37.

Flaw Parameters							Detection Values	
Flaw No.	Location	Shape	Method	Long. Dim. (mm)	Circ. Dim. (mm)	Depth Dim. (mm)	Radial Amplitude	Radial Duration (mm)
26	external	RB	EDM	2.38	2.38	1.20	55.1	4.0
27	internal	RB	EDM	2.38	2.38	1.19	32.1	5.4
28	internal	RB	EDM	2.08	2.05	0.61	8.4	4.2
29	external	RB	EDM	2.06	2.04	0.60	16.4	3.9
30	external	FB	EDM	2.38	2.38	1.30	57.5	4.9
31	internal	FB	EDM	2.38	2.38	1.30	43.9	5.3
32	internal	FB	EDM	2.38	2.38	0.58	20.6	5.0
33	external	FB	EDM	2.38	2.38	0.58	37.1	3.9
34	external	cone	EDM	2.20	2.15	1.10	36.3	3.6
35	internal	cone	EDM	1.96	1.91	0.98	29.0	4.2
36	internal	cone	EDM	0.95	0.94	0.47	4.0	2.1
37	external	cone	EDM	1.31	1.29	0.66	9.8	3.4

that the sensor head be designed to severely restrict the amount of liftoff.

Acknowledgements We gratefully acknowledge the partnership of the University of Tulsa and the University of Tulsa Coiled Tubing Mechanics Research Consortium in the project. This work was supported by the Office of Fossil Energy, U.S. Department of Energy, under the Department of Energy's Idaho Operations Office Contract DE-AC07-05ID14517.

References

[1] A. Sas-Jaworsky II, M. E. Teel (Eds.), Coiled Tubing Handbook, Gulf Publishing Company, 1993.

[2] R. K. Stanley, Overview of the nondestructive inspection techniques for the evaluation of coiled tubing and pipe, Materials Evaluation 54 (11) (1996a) 1245–1250.

[3] R. K. Stanley, Observations on magnetic wall measurements of coiled oilfield tubing, Materials Evaluation 62 (2) (2004) 125–128.

[4] L. Smith, J. Misselbrook, An overview of inspection technology

Table 6
Geometry, method, and the detected signal amplitudes and durations of artificial flaws in TU flaws 38-49.

Flaw Parameters							Detection Values	
Flaw No.	Location	Shape	Method	Long. Dim. (mm)	Circ. Dim. (mm)	Depth Dim. (mm)	Radial Amplitude	Radial Duration (mm)
38	external	RB	EDM	2.38	2.38	1.21	50.7	3.9
39	internal	RB	EDM	2.38	2.38	1.21	29.0	4.6
40	internal	RB	EDM	2.02	2.02	0.58	9.2	4.5
41	external	RB	EDM	2.05	2.02	0.58	16.3	4.0
42	external	FB	EDM	2.38	2.38	1.22	61.1	4.4
43	internal	FB	EDM	2.38	2.38	1.13	36.1	5.3
44	internal	FB	EDM	2.38	2.38	0.75	15.6	5.2
45	external	FB	EDM	2.38	2.38	0.73	35.9	4.0
46	external	cone	EDM	2.38	2.38	1.23	38.0	4.1
47	internal	cone	EDM	2.38	2.38	1.23	24.6	4.62
48	internal	cone	EDM	N/A	N/A	0.61	5.8	4.0
49	external	cone	EDM	N/A	N/A	0.61	7.0	3.9

and criteria for inspecting coiled tubing, in: 2nd North American Coiled Tubing Roundtable, Montgomery, Texas, 1997.

[5] S. M. Tipton, Multiaxial plasticity and fatigue life prediction in coiled tubing, in: M. R. Mitchell, R. W. Landgraf (Eds.), Fatigue Lifetime Predictive Techniques: 3rd Volume, ASTM STP 1292, American Society for Testing and Materials, 1996, pp. 283–304.

[6] J. G. Proakis, D. G. Manolakis, Digital Signal Processing: Principles, Algorithms, and Applications, 2nd Edition, Macmillan, Macmillan Publishing Company, 866 Third Ave., New York, NY 10022, 1992.

[7] L. W. I. Couch, Digital and Analog Communication Systems, 4th Edition, MacMillan, 1993.

[8] K. Hwang, S. Mandayam, S. S. Udpa, L. Udpa, W. Lord, M. Atzal, Characterization of gas pipeline inspection signals using wavelet basis function neural networks, NDT&E International 33 (2000) 181–188.

[9] S. Cholowsky, S. Westwood, Tri-axial and 3-dimensional magnetic modelling of defects combine to improve defect sizing from magnetic flux leakage signals, in: NACE International Northern Area Western Conference, 2004.

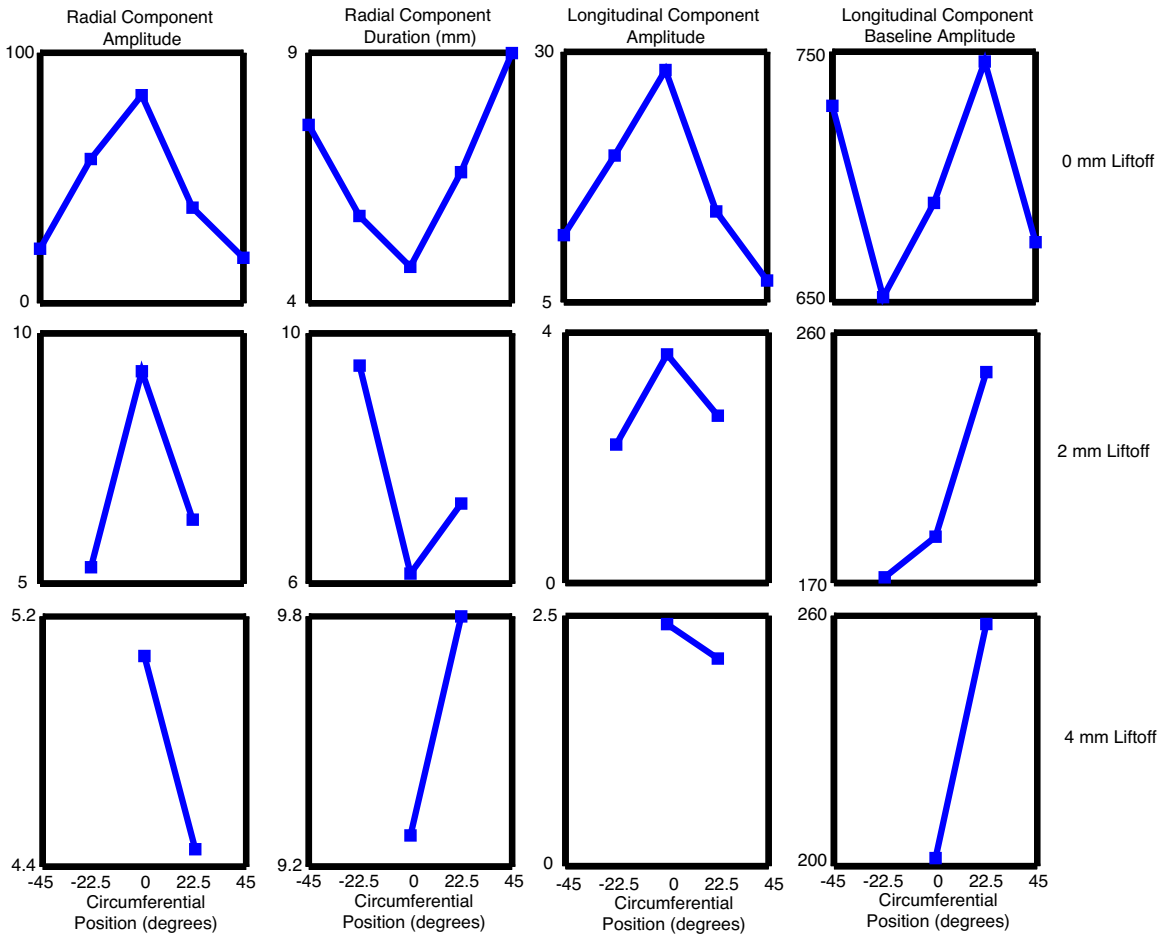

Fig. 7. Additional effects of liftoff on the signals of the radial and longitudinal sensors. A summary of the characteristics of the signal for Flaw 5 on CT2 are shown. The results are plotted versus the circumferential position of the five sensors.